Technische Universität München
TUM School of Medicine and Health

Investigation of the Effect of Nano Particles Containing Ac2-26 on Intestinal Inflammation in the Context of Inflammatory Processes in the Intestine

Joseph Raphael Elias Miltschitzky

Vollständiger Abdruck der von der TUM School of Medicine and Health der Technischen Universität München zur Erlangung eines

Doktors der Medizinischen Wissenschaft (Dr. med. sci.)

genehmigten Dissertation.

Vorsitz: apl. Prof. Dr. Klaus-Peter Janssen

Prüfende der Dissertation:

1. Priv.-Doz. Dr. Philipp-Alexander Neumann
2. Prof. Dr. Hana Algül
3. Priv.-Doz. Raquel Mejias-Luque, Ph.D.

Die Dissertation wurde am 28.02.2024 bei der Technischen Universität München eingereicht und durch die TUM School of Medicine and Health am 09.10.2024 angenommen.

Technische Universität München

Investigation of the Effect of Nano Particles Containing Ac2-26 on Intestinal Inflammation in the Context of Inflammatory Processes in the Intestine

Wissenschaftliche Arbeit zur Erlangung des Grades

Dr. med. sci.

an der TUM School of Medicine and Health der Technischen Universität München.

Betreuer/-in	Dr. med. Stefan Reischl Institut für diagnostische und interventionelle Radiologie am Klinikum Rechts der Isar
Aufgabensteller/-in	PD Dr. med. Philipp-Alexander Neumann Klinik und Poliklinik für Chirurgie am Klinikum Rechts der Isar
Eingereicht von	Joseph Raphael Elias Miltschitzky elias.miltschitzky@tum.de
Eingereicht am	München, den 28.02.2024

Table of Contents

1. Introduction

In abdominal surgery, delayed or insufficient healing at the site of a colorectal anastomosis is a complication that can lead to anastomotic leakage (AL) and thus significantly increase morbidity and mortality of patients (Peeters, Tollenaar et al. 2005, Thompson, Chang et al. 2006, Krarup, Nordholm-Carstensen et al. 2014, Gessler, Eriksson et al. 2017) and even increases the rates of cancer recurrence (Law, Choi et al. 2007). Patients with AL require reoperation in many cases (Choi, Law et al. 2006) and this often results in the patient to be left with a permanent stoma (Khan, Wheeler et al. 2008). The incidence of AL is far from infrequent, for example, (Paun, Cassie et al. 2010) showed a worldwide incidence of AL of 11% in rectal cancer patients undergoing radical surgery. Various other publications report rates of 1 – 24% in patients requiring colonic or rectal anastomoses, depending on patients' conditions, location of the anastomosis, surgical specialization and others (Smith, King et al. 2003, Matthiessen, Hallbook et al. 2007, Krarup, Jorgensen et al. 2012, Krarup, Nordholm-Carstensen et al. 2014, Pommergaard, Gessler et al. 2014, McDermott, Heeney et al. 2015). Findings like this serve to illustrate that AL is a complication of major clinical relevance and accounts for huge healthcare costs (McDermott, Heeney et al. 2015). Despite several decades of focused research, there are still too many unknowns and no clinically approved therapy to improve healing and prevent AL has emerged yet (Nerstrom, Krarup et al. 2016). To a huge degree this is due to gaps in our knowledge of the complex, orchestrated gastrointestinal healing processes. Since this healing process can depend on local and systemic factors as well as the surgical technique, nutritional factors (Mukherjee, Kavalukas et al. 2016) and local microbiota (van Praagh, de Goffau et al. 2016, Bachmann, Leonard et al. 2017), and since clinical studies can only assess clinical outcomes retrospectively (Marjanovic and Hopt 2011), the only insights can be gleamed from experimental studies.

1.1. Physiology of anastomotic healing

1.1.1. Overview of intestinal healing

Anastomotic healing proceeds in a pattern common to all healing processes which can be divided into four different stages (DiPietro 1995): hemostasis; the inflammatory phase, in which the main immunologic response to pathogens, debridement and provisional wound closure take place; the proliferative phase, characterized by synthesis of collagen,

angiogenesis and re-epithelialization and, finally, the regenerative phase finalizing the healing process by reorganizing the scar tissue (Rijcken, Sachs et al. 2014).

Immediately after an injury to the mucosa, the wound is flushed clean by extravasation of blood from damaged blood vessels or transudation of fibrinogen-rich fluid with platelets and other coagulation factors from a rapidly forming oedema (Marjanovic and Hopt 2011). In bleeding wounds (also in surgically adapted wounds) activated blood platelets aggregate and form an unstable, whitish clot and thus seal the wound provisionally (primary hemostasis). The second phase of wound closure (secondary hemostasis) is dependent on blood borne proteins and can be subdivided into two different pathways merging at the end to polymerize and cross-link fibrin fibers. The combination of these fibers and the primary white clot form a more stable, reddish clot, sealing off the wound effectively.

The coagulation cascade serves not only to seal the wound, but is also tied in closely with triggering an immediate immune response through complement activation (Weidmann, Heikaus et al. 2017) and production of bradykinin which binds to B_1 and B_2 kinin receptors to trigger inflammation (Weidmann, Heikaus et al. 2017). Studies suppressing this inflammatory response have shown that it is vital to the healing process, since suppression of inflammation slows down the healing process and weakens anastomotic strength (Del Rio, Beck et al. 1996, Mantzoros, Kanellos et al. 2006, Inglin, Baumann et al. 2008, Zacharakis, Demetriades et al. 2008).

In concert with coagulation, coordinated recruitment of leukocytes helps mount an effective defense against pathogens and to release tissue mediators. Recruited by complement protein C3a (Wu, Brennan et al. 2013), neutrophils are the first responders at the site of injury (Witte and Barbul 1997, Engelhardt, Toksoy et al. 1998, Martin and Leibovich 2005). However, they are a “double edged sword” (Leoni, Neumann et al. 2015) since a fine balance between their beneficial and detrimental effects on wound healing needs to be maintained. While suppression of neutrophil activation and invasion hampers healing under most non-sterile conditions, excessive activation has been reported in chronic inflammations (Xavier and Podolsky 2007, Fournier and Parkos 2012). Neutrophils scavenge cellular debris and produce reactive oxygen species (ROS) and several cytokines. ROS presence has also been shown to be important for macrophage recruitment (Tauzin, Starnes et al. 2014). They are the next population of leucocytes taking over from the neutrophils by migrating into the tissue surrounding the injury, phagocytose apoptotic neutrophils (Ortega-Gomez, Perretti et al. 2013), other dead cells and debris (Witte and Barbul 1997, Chen and Nunez 2010). They stimulate neutrophil

apoptosis (Ortega-Gomez, Perretti et al. 2013) and reverse migration. These processes have been subsumed under the term “neutrophil resolution” (Tauzin, Starnes et al. 2014). Macrophages are the predominant cell species in the wound bed two to four days after an injury (Witte and Barbul 1997) and differentiate into so-called “wound-associated macrophages”. Classically, two antagonistic macrophage sub-populations can be distinguished: the inflammatory monocytes can differentiate into activated, M1 macrophages producing proteases (Chen and Nunez 2010), NO (Murray and Wynn 2011), inflammatory cytokines (Chen and Nunez 2010, Barron and Wynn 2011, Murray and Wynn 2011, Sindrilaru, Peters et al. 2011), whereas the tissue-resident M2 macrophages maintain epithelial homeostasis (Murray and Wynn 2011, Leoni, Neumann et al. 2015), moderate inflammation by secreting anti-inflammatory factors (Murray 2005, Leoni, Neumann et al. 2015) and stimulate epithelial proliferation and production of collagen (Barron and Wynn 2011). However, a certain plasticity in macrophage differentiation has been observed, enabling macrophages to switch subtype if required (Biswas and Mantovani 2010, Murray and Wynn 2011). Just like in neutrophils, there is evidence that a very delicate balance needs to be maintained lest the amount of macrophages present at the site of injury can be detrimental to a successful wound healing (Sindrilaru, Peters et al. 2011).

Also, in addition to these two populations of leukocytes, an important role for mast cells in the immediate mounting of an immune response has been postulated (Martin and Leibovich 2005).

This influx of macrophages overlaps with the proliferative phase (DiPietro 1995) and definite wound closure which take place from the 2nd to 14th day after injury (Rijcken, Sachs et al. 2014). Here, fibroblasts and endothelial cells are the predominantly proliferating cell populations (Witte and Barbul 1997). Several studies have identified the cytokine annexin A1 (ANXA1) that is secreted by activated and apoptosing polymorphonuclear neutrophils (PMNs) (Scannell, Flanagan et al. 2007, Bratton and Henson 2011) as an important mediator for this transition (Bratton and Henson 2011) which is required for a timely resolution of acute or chronic inflammation (Yang, Morand et al. 2004, Leoni, Neumann et al. 2015). In addition to re-epithelialization, cell proliferation, extra-cellular matrix (ECM) reformation and angiogenesis take place during this proliferative phase. On the fourth postoperative day, fibroblasts represent the most dominant cell population in the area of wound healing (Rijcken, Sachs et al. 2014). They replace the provisional ECM formed by coagulation with granulation tissue and day 6 sees the critical switch from net collagen uptake to collagen deposition and thus ECM synthesis (Migaly, Lieberman et al. 2004).

Angiogenesis is induced by local hypoxia and presence of NO secreted by leukocytes as well as chemokines such as monocyte chemotactic protein-1 (MCP-1) and macrophage inflammatory protein (MIP-1a). However, excessive angiogenesis is prevented by a variety of endogenous angiogenesis inhibitors, such as thrombospondin (TSP-1), interferon gamma (IFN-g), interferon gamma-induced protein-10 (IP-10), interleukins 4 and 12, and tissue inhibitors of matrix-metalloproteases (TIMPs). Around the 7th day after injury, T-lymphocytes migrate into the wound and seem to prevent excessive tissue growth (DiPietro 1995).

This proliferative phase is followed by the remodeling phase, which can last for months to years even and is comparatively poorly researched and often excluded by experiments conducted on shorter timespans. Fibrillar collagen is slowly degraded, rebuilt, and maturated. Crosslinking of fibrillar collagen provides increasing mechanical strength. This requires a delicate regulatory balance of matrix-metalloproteases (MMPs) and TIMPs. In addition to that, the severed layers of the intestinal wall reorganize. The regression of vascularization to normal levels marks the final transition to mature scar tissue.

1.1.2. Pathophysiology of AL and criteria for successful anastomotic healing

When talking about pathological anastomotic healing leading to AL, one must define criteria for insufficient healing. A definition given by (Dubay and Franz 2003) considers a wound healing failure “an interruption in the timely recovery of the injured tissue’s mechanical integrity”. AL can occur if any critical component of the physiological processes leading to closure of the intestinal wound is disrupted. It goes without saying that interruption of continuity of the healing tissue disrupts the entire healing process. Therefore, until the anastomosis has regained enough tensile strength, success of the healing process is entirely dependent on the mechanical apposition by suture (Dubay and Franz 2003) or stapler. (Thompson, Chang et al. 2006) has described a sigmoid-shaped curve for tensile strength plotted versus time after surgery, starting with an early “lag-phase” corresponding to the inflammatory phase. When considering the relative incidence of AL, it is highest during this phase which may be due to the high collagenase activity resulting in a reduction of strength of up to 70% within the first 48 hours (Thornton and Barbul 1997). During the first three to five days, cohesion of the anastomosis relies entirely on suture materials (Migaly, Lieberman et al. 2004). Insufficient hemostasis due to platelet defects, lack of soluble factors or bad surgical technique can cause hematoma and thus prevent proper formation of the provisional ECM (Dubay and Franz 2003). Also, mounting an insufficient immune response can lead to a defective healing process. Suppressing inflammation via anti-inflammatory drugs such as corticosteroids or non-steroidal

anti-inflammatory drugs (NSAIDs) have been shown to impair normal anastomotic healing. Conversely, a perpetuated inflammatory phase (as seen in patients afflicted with ulcerative colitis or Crohn's disease) has been reported to prevent the tissue from proceeding to the later phases of wound healing (Dubay and Franz 2003).

Another important step towards sealing over a defect is re-epithelialization. In small wounds, epithelial sheet migration and contraction of actin-myosin cytoskeleton is adequate to cover the exposed wound bed, whereas in larger defects the epithelium has to proliferate to provide enough cells (Leoni, Neumann et al. 2015). In case of an anastomosis, the surgical incision not only interrupts the epithelium, but severs all layers of the intestine. The best way to surgically adapt the two stumps in an anastomosis has been the subject of study in surgery for more than a century and there still is no universally accepted method. However, there is a consensus in literature that oxygenation of the healing tissue is essential and therefore ischemia must be avoided at all costs. In an "ideal" end-to-end anastomosis, the two stumps are neatly fused together without mechanical tension on the anastomosis and without impediments to perfusion. This requires mobilization of the intestine without disrupting blood vessels supplying the anastomosis (Thornton and Barbul 1997). Perfusion might be compromised through tight stapling or suturing as well as in patients with hypovolemia, hypotension or shock (Dubay and Franz 2003). In addition, the different layers of gastrointestinal tissue need to be adequately adapted. However, there is still a controversy going on about which layer should be used to mechanically adapt the anastomosis, if sutures or stapling should be preferred, if the anastomosis needs to be protected from the passage of food by a proximal ileo- or colostomy (Sharefkin, Joffe et al. 1978), if peritoneal cover is a protective factor or not (Goligher, Graham et al. 1970, Sharefkin, Joffe et al. 1978) or where to place the omentum (Sharefkin, Joffe et al. 1978). Traditionally, an inverting suture (Thornton and Barbul 1997) within the submucosa (Thornton and Barbul 1997, Thompson, Chang et al. 2006) is used to effect a direct apposition, avoiding mucosal inversion or eversion. (Thornton and Barbul 1997) has identified the serosa as a vital layer to avoid AL when appositioned directly. Fibrin glue and wrapping anastomoses with biodegradable materials or pericardium to improve their stability are explored as novel therapeutic approaches but have not found their way into routine clinical practice.

1.2. Pro-resolutory mediators of inflammation and their receptors

1.2.1. The formyl peptide receptor family: a class of GPCRs

Formylated peptides such as formyl-methionyl-leucyl-phenylalanine (fMLP) are bacterial products which serve as powerful chemoattractants during an infection, recruiting leukocytes which express suitable receptors to the site of infection (Le, Li et al. 2000). There are high-affinity fMLP receptors, namely formyl-peptide receptor type 1 and 2 (FPR1 and FPR2/ALX) as well as the low-affinity, so-called formyl peptide receptor-like receptors FPRL1 and FPRL2 (Le, Li et al. 2000). They all belong to the seven-transmembrane domain G_i-protein-coupled receptor family (Babbin, Lee et al. 2006). Upon ligand binding, multiple internal downstream signaling cascades are activated (Rane, Carrithers et al. 1997, Perretti 1998, Belisle and Abo 2000, Glogauer, Hartwig et al. 2000, Le, Li et al. 2000, Roviezzo, Getting et al. 2002, Chodniewicz and Zhelev 2003) to induce production of acute phase reactant proteins (Babbin, Lee et al. 2006) and at higher concentrations (which probably occur at the site of an inflammation), FPR(L) ligand binding can trigger production of ROS (Rescher, Danielczyk et al. 2002) and neutrophil degranulation (Belisle and Abo 2000). Leukocytes and epithelial cells have also been shown to exhibit an increased motility under the influence of FPR(L) activation by bacteria-derived ligands (VanCompernolle, Clark et al. 2003). These cumulative effects seem to enable leukocytes to rapidly track down and attack microbes.

Experiments showing an increase in filamentous actin content in epithelial cells and fibroblasts upon FPR(L) stimulation (Rescher, Danielczyk et al. 2002, VanCompernolle, Clark et al. 2003) suggest that an effect similar to that in leukocytes (see above) leads to increased motility in these cells. The physiological function of this increase in motility of fibroblasts might be to enable epithelial cells and fibroblasts to migrate towards the site of an injury where microbes are present and thus promote rapid re-epithelialization and ECM synthesis. Considering the experimental pro-resolution properties of many FPR(L) ligands and their release at the site of inflammation in healing tissues (see below) can only reinforce this hypothesis that FPR(L)s activation is vital to successful healing of wounds.

However, (Le, Li et al. 2000) reported that FPR(L) activation also leads to its desensitization. Apart from the abovementioned bacterial peptides, there are endogenous ligands for fMLP receptors which can be roughly classified into annexins and lipid, so-called “specialized pro-resolution mediators” (SPMs), which exert a different, anti-inflammatory

and pro-resolution-of-inflammation effect along the same pathways. A full, in detail analysis of the intertwined pathways and regulation of SPM biochemistry can hardly be the scope of this thesis, however, especially since the decision was made to focus on ANXA1 as a test substance for the model system examined here (see 1.3).

1.2.2. Annexins

Annexin A1 (ANXA1, also known under its former name lipocortin 1), which is secreted by activated and apoptosing polymorphonuclear neutrophils (PMNs) (Scannell, Flanagan et al. 2007, Bratton and Henson 2011) through limited proteolysis, could be shown to interact with the FPR2/ALX GPCR. Additionally, it's N-terminally derived peptide Ac2-26 interacts with formyl peptide receptor-like 1 receptor (FPRL1) (Perretti, Chiang et al. 2002), and all three known receptors in the FPR-family (Hughes, Becker et al. 2017). This affinity of the N-terminal peptide suggests that it is indeed the N-terminus of ANXA1 that is responsible for successful binding of the full-length peptide (Babbin, Lee et al. 2006).

ANXA1 has been shown to mediate inflammatory response (Sheikh and Solito 2018) and promotion of epithelial wound repair in experimental (Leoni, Alam et al. 2013) and clinical (Leoni, Neumann et al. 2015) settings. Receptor binding by Ac2-26 inhibits downstream signaling and activation of membrane phospholipase A_2 with consequent pro-inflammatory eicosanoid synthesis and could be shown to start an intracellular ROS-signaling cascade in epithelial cells. This increase in ROS leads to increased epithelial cell motility (Leoni, Alam et al. 2013). These effects seems to mediate some of the anti-inflammatory effects of glucocorticoid hormones (Perretti 1998, Roviezzo, Getting et al. 2002). It has also been shown to inhibit the recruitment and extravasation of PMNs (Perretti, Croxtall et al. 1996) and enhances their non-phlogistic phagocytosis by macrophages in concert with apoptosis (this process of "carrying a cell to the grave" is called efferocytosis (Bratton and Henson 2011)). Additionally, it has been shown to promote apoptosis of surrounding PMNs (Solito, Kamal et al. 2003).

Another interesting result was found by (Rescher, Danielczyk et al. 2002): ANXA1 release can be stimulated by Ac2-26 binding in epithelial cells. This suggests an autocrine signaling mechanism with a positive feedback mechanism.

1.3. Development of a standardized mouse model to study anastomotic healing during inflammatory conditions

When confronted with the multitude of different pro-resolutory mediators, the obvious (and of course, highly relevant) question is: which one works best in which setting? It is hard to give any kind of ranking as to the potency of these molecules since there are no comparative analyses pitching different mediators against each other in a standardized setting. The difficulty in comparing different studies on the various mediators validly is to a large part caused by different approaches and the non-standardized reporting quality of many animal experiments (Yauw, Wever et al. 2015). There is also a low number of studies on anastomotic healing during inflammatory conditions (Yauw, Wever et al. 2015). All this highlights the need to develop a standardized model which objectivizes findings for assessing the various mediators under comparable conditions.

The combination model of experimental colitis and colorectal surgery developed and presented in this thesis is a feasible and adaptable platform for this kind of research.

Although historically most studies have been performed in rats and dogs (Yauw, Wever et al. 2015), mice seem to be the most appropriate model organism to examine anastomotic healing (Pommergaard, Rosenberg et al. 2011). It is much easier to induce anastomotic leakage in mice (Pommergaard, Rosenberg et al. 2011) and the intraabdominal intestinal immune response in mice is more comparable to humans (Pommergaard, Rosenberg et al. 2011). Mice are cheaper and easier to handle and the wide variety of available knockout genotypes in mice offers the possibility to research the influence of an immense number of factors on anastomotic healing. The BALB/c strain is recommended due to its high susceptibility to the experimental DSS-colitis. The surgical approach presented here was designed to avoid ischemia as a confounding factor in development of anastomotic leakage by sparing all vessels, as research on anastomotic perfusion is not the scope. Tissue-specific targeting (see 2.1.1) allows for precise introduction of the mediator of choice into the desired region and metabolic pathway.

But any such model must withstand a real-life-test. In this thesis, the model is applied to test the effect of one pro-resolutory mediator as a proof-of-concept. Due to the promising results presented above (see 1.1.1 and 1.2.2), Ac2-26 was selected as a suitable candidate. Having established our model, the groundwork is laid for sequential testing of different mediators – an endeavor which is beyond the scope of this thesis, however.

2. Materials and Methods

2.1. Materials

2.1.1. Nanoparticles (Reischl, Lee et al. 2021)

To affect a tissue-targeted delivery of the Ac2-26 molecule, the active compound was coated in a shell of collagen IV fibers. Collagen IV receptors are primarily expressed in tissue where matrix-restructuring processes take place – like at the site of anastomotic healing. This makes collagen IV nano-shells an ideal targeting marker for the purpose of this research endeavor. The nanoparticle was dubbed Ac2-26-NP in our experimental protocols.

To control for an effect the collagen IV or the individual amino acids which Ac2-26 consists of could exert on the healing process, a control nanoparticle was synthesized of the same collagen IV shell as the Ac2-26-NP around an oligopeptide with the same amino acids as Ac2-26, however in a scrambled sequence. This particle was dubbed Scrm-NP and used for sham treatment (see 2.2.1).

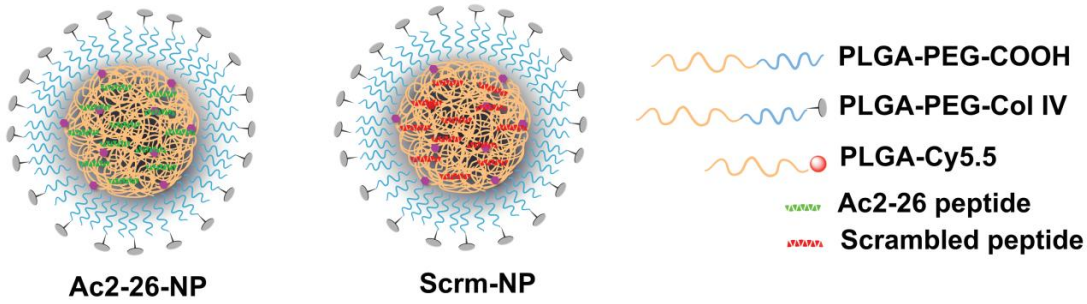

Figure 1: Schematic molecular structure of Ac2-26- and Scrm-NP.
Adapted Figure 3a from (Reischl, Lee et al. 2021)

2.1.2. Other surgical and lab materials

A full list of all materials used has been included in the appendix.

2.2. Methods

2.2.1. Experimental groups and encoding

To easily catalogue mice, a six-digit, hyphenated labelling code was devised and assigned to each animal:

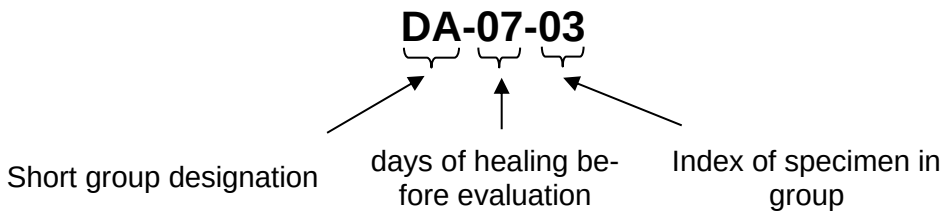

The mice themselves were ear-marked with running numbers and a chart containing both the ear-mark-number and the coding was kept as the basis for all data acquisition. Groups and animals were then randomized for surgery to avoid any bias, i.e., through improving surgical skill during the experiment.

Group sizes were selected based on a statistical analysis conducted by the Institute for Medical Informatics, Statistics and Epidemiology at Technical University of Munich in 2017 (Ulm 2017). Using non-parametrical Mann-Whitney-U-test and assuming a clinically relevant difference in histopathological score between groups, an effect of P(Y<X) = 0.129 can be calculated. This means that 10 individuals must be analyzed to achieve a power of 80% for detecting differences between groups on a 5% significance level.

The number of reserve animals was calculated based on yet unpublished data from previous experiments in the lab: In 5% of experiments, DSS colitis may not develop sufficiently, therefore the animals must be taken out of the experiment prematurely. In another 5% of experiments, intraoperative complications such as excessive blood loss or anesthetic overdosing may lead to premature abort of the experiment. In about 5% of successfully conducted experiments, technical difficulties in sample analysis made obtaining valid data impossible. This means that an average of $95\%\text{x}95\%\text{x}95\% = 85.73\%$ of experiments yield valid data, or

$$n_{valid} = 0.8573 * n_{total}$$

where n_{valid} is the desired number of successful experiments and n_{total} is the required number of animals to start with. This means, that

$$n_{total} = \frac{n_{valid}}{0.8573} = 116.6\% * n_{valid}$$

This shows that for an average of 10 animals to reach the defined endpoints and yield valid data, the experiment needs to be started with at least 12 animals for each group.

Designation	Days before evaluation	Number of Animals	Description
D2	7	6	Dose finding for DSS-colitis, 2%
D3	7	30	Dose finding for DSS-colitis, 3%
D5	7	14	Dose finding for DSS-colitis, 5%
H0	3, 7, 14	12	Control group; surgery without DSS-colitis or treatment
D0	3, 7, 14	12	Control group; DSS-colitis with 5% followed by surgery, no treatment. **Aborted after the first 14 experiments due to excess inflammation and insupportable complication rate**
DX	3, 7, 14	12	Control group; DSS-colitis with 2% followed by surgery, no treatment
DS	3, 7	12	Control group; DSS-colitis with 2% followed by surgery, sham treatment by i.p. injection of Scrm-NPs. **Operated and evaluated by the next doctoral candidates in the lab, R. L. Walter and V. Vieregge**
DA	3, 7, 14	12	Experiment group; DSS-colitis with 2% followed by surgery, treatment with i.p. injection of Ac2-26 NPs

Table 1: List of groups
Own table based on group design.

2.2.2. Monitoring and abort criteria

Modified from (Miltschitzky, Clees et al. 2021).

Mice were scored daily based on clinical aspects of post-operative healing as well as national and lab-internal animal welfare regulations. The scoring protocol including the criteria listed in Table 2 and the following algorithm for therapeutic measures and abort criteria was used:

- at a score of 0 no measures were considered necessary
- at a total score of 1 to 3 therapeutic measures were considered (consisting of analgesia, antibiotic treatment, substitution of moistened chow, hydrogel or i.p. fluid as applicable)
- at a total score of 4 to 8 an immediate report to the veterinarian oversight was made and therapeutic measures were taken mandatorily
- at a total of more than 8 score points or any single score of 4 the experiment was aborted, and the animal euthanized immediately (see 2.2.7.1)

Criteria	Score points
Weight	0= No reduction
	1= Reduction of 0-5%
	2= Reduction of 6-10%
	3= Reduction of 11-19%
	4= Reduction of >19%
Fur	0= Normal, shiny, smooth
	1= Piloerection
Behavior	0= Normal
	1= Subdued, no exploration, reduced interaction
	4= Apathy, isolation, stereotypic behavior
Posture	0= Normal
	2= Intermittent cowering or shivering
	4= Permanent cowering or shivering
Pain	0= No indication
	2= Defensive behavior on palpation of abdomen
Impaired wound healing	0= No indication
	2= Red or oozing wound
	4= Dehiscent suture or ruptured abdomen
Dehydration	0= Skin folds straighten within 2s
	1= Persistent skin folds
Mucous membranes (Ears, skin, extremities)	0= Rosy
	1= Pale
Stool	0= Formed
	1= Diarrhea

Table 2: Scoring protocol for daily assessment of mouse health
Table 1 from (Miltschitzky, Clees et al. 2021).

During induction of DSS colitis, the continuous uptake with drinking water provokes a mid-grade inflammation of the intestinal mucosa, which was monitored by daily determination of the disease activity index (DAI). The animals were weighted daily, the stool was examined regarding its consistency and tested for occult rectal bleeding using a hemoccult-test.

Postoperative animals received analgesia (see 2.2.4) until the second postoperative day. On POD2 an additional hemoccult-test was added to the scoring routine.

2.2.3. Dextran sodium sulphate induced colitis (DSS-colitis)

Modified from (Miltschitzky, Clees et al. 2021).

For induction of DSS-colitis, the protocol published in (Wirtz, Neufert et al. 2007) and it's 2017 revision (Wirtz, Popp et al. 2017) was used. This experimental setting simulates the healing processes in post-inflammatory intestinal mucosa that can also be found in human patients with chronic inflammatory bowel disease (IBD).

We conducted preliminary dose-finding experiments using the D2, D3 and D5 group. The target was an inflamed, but not completely ulcerated mucosa. This prevents excessive weight loss, a high disease activity and high strain on the animals.

The desired dosage of DSS was mixed into the *ad libitum* drinking water of the mice and provided to them for seven days. After this period, the drinking water with DSS was exchanged for normal water to induce healing.

2.2.4. Anesthesia and analgesia

Modified from (Miltschitzky, Clees et al. 2021).

Anesthesia for all procedures was induced by immersing the mouse completely into a chamber flooded with 2 up to 5% of isoflurane with 3L/min of oxygen as a carrier gas. After the transition through Guedel's excitation state, positional reflexes were tested. If no reflectory rolling back into a prone position after rolling the animal onto it's back could be seen, the mouse could be positioned for the planned procedure (in a prone position for coloscopy or supine for surgery). To sustain anesthesia, the mouse's nose was placed into a respirator mask connected to the ventilation machine with 1.5 up to 2% of isoflurane at an oxygen flow of 1L/min.

Due to relaxation, no blinking occurs during general anesthesia and the animal's natural temperature regulation is suppressed. This can lead to exsiccation of the exposed corneas and dangerous hypothermia. To protect the cornea in absence of blinking, eyes were covered in Bepanthen© salve. To avoid hypothermia, a heating pad was placed on the operating surface. However, the tail is particularly sensitive to heat, which can cause postoperative oedema and necrosis. To avoid these complications, the tail had to be isolated by cellophane or cork to reduce local temperature to between 26 to 30°C.

No further analgesia was needed for colonoscopy or euthanasia. To provide a sufficient analgesic effect for surgical tolerance, the inhalation anesthesia was combined with oral and injection analgesia by administration of 1 drop of a 500 mg/ml metamizole solution per kg live weight orally and 1 mg/kg live weight of Metacam s.c. 20 minutes prior to isoflurane application. Surgical tolerance was then tested by checking the paw reflex: no reflectory withdrawal of the extremity may occur upon squeezing a mouse's hind paw with blunt pliers.

For postoperative pain management, three injections of buprenorphine 0.1 mg/kg live weight s.c. were applicated on the day of surgery, as well as an additional dose of 1 mg/kg live weight of Metacam s.c. on each the first and second post-operative day.

Post-operatively, isoflurane anesthesia does not need to be antagonized. For better post-operative recovery, each mouse was held in hand to warm it while awakening.

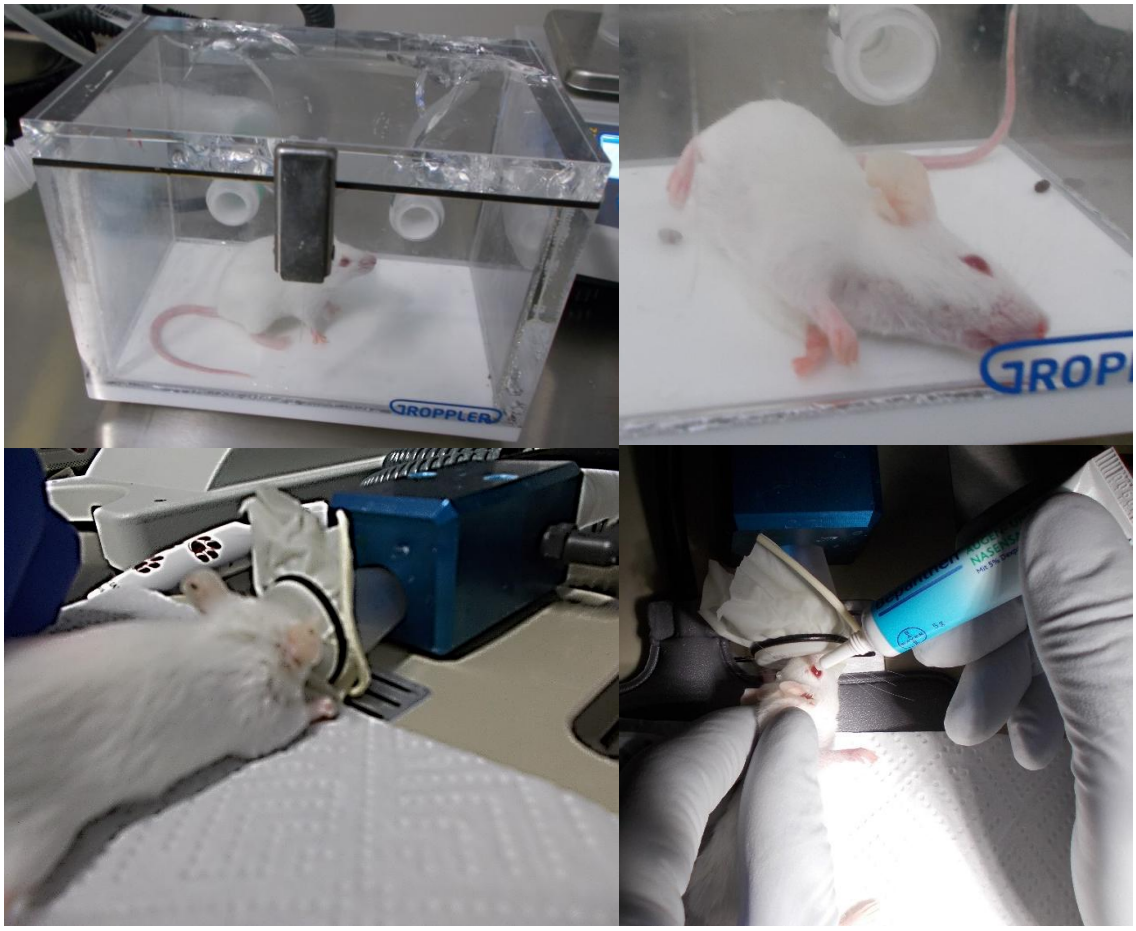

Figure 2: Induction of anesthesia.
Top left: mouse in induction chamber before induction of anesthesia.
Top right: after induction with 5% isoflurane and 3L/min flow, positional reflexes are lost. Bottom left: to sustain anesthesia, the nose of the mouse is placed into a respirator with a steady flow of isoflurane. Bottom right: to avoid the corneas from drying out, Bepanten© salve is applied.
Modified from the supplement of (Miltschitzky, Clees et al. 2021).

2.2.5. Coloscopy

Modified from (Miltschitzky, Clees et al. 2021).

Murine coloscopy has been an established method for assessment of intestinal inflammation in mice for a couple of years. Here, a murine endoscope developed by the Karl Storz company was used to assess the state of the mucosa resp. the state of the mucosa and anastomosis directly *in vivo* before surgery and before evaluation.

Following induction of anesthesia (see 2.2.4), the anus was lubricated with a drop of local anesthetic gel (Instillagel®). The endoscope was inserted under careful insufflation of

0.9% saline solution and advanced up to the colon flexure, then the video recording for standardized evaluation was started while pulling back steadily until exiting from the colon.

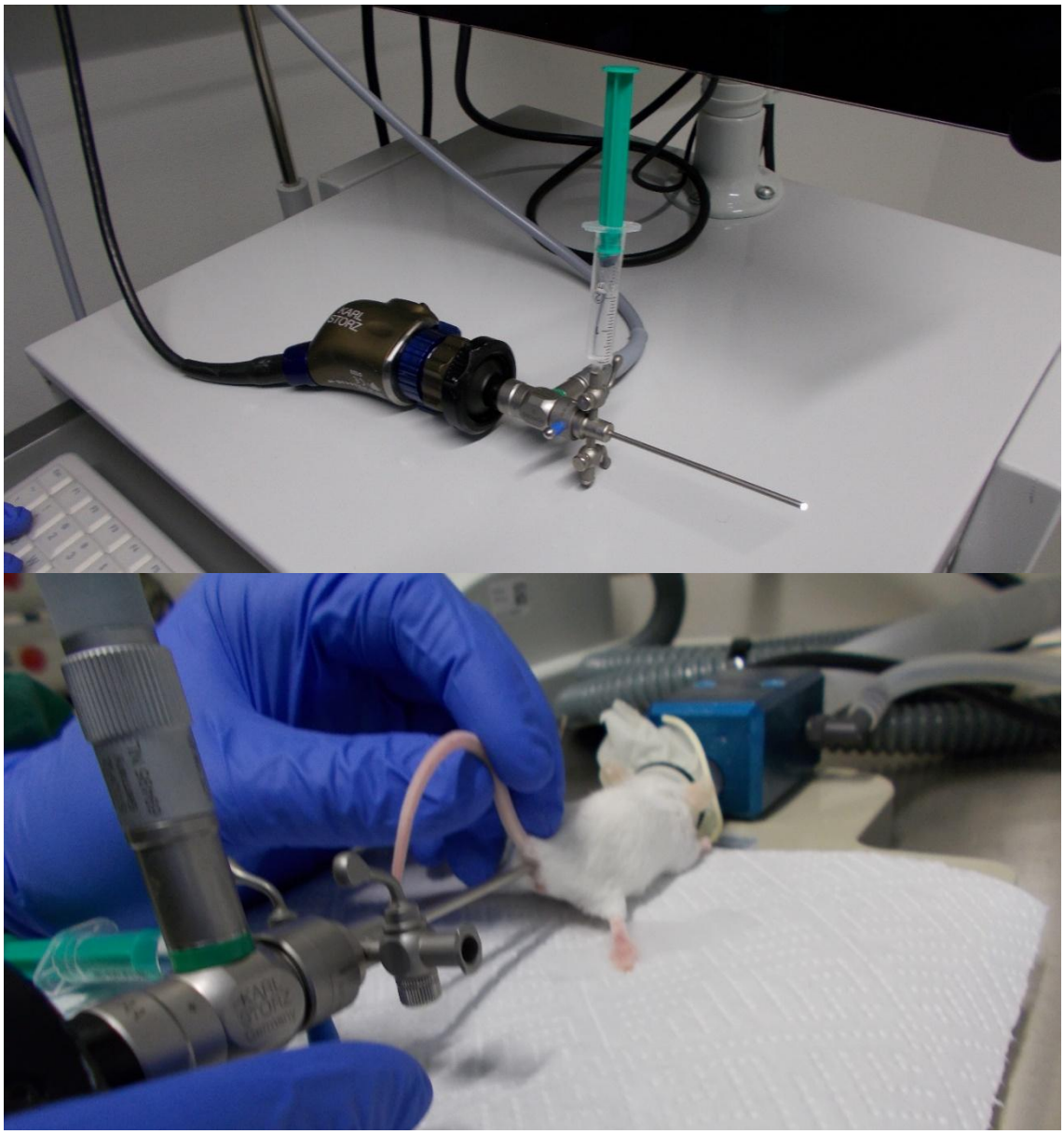

Figure 3: Colonoscopy.
Top: Colonoscopy assembly. 0.9% sodium chlorine solution is used as a medium for inflation of the bowel. Bottom: coloscopy on mouse in supine position, nose in the respirator. The stiff murine colonoscopy can easily be inserted and advanced up to the colonic flexure.
Modified from the supplement of (Miltschitzky, Clees et al. 2021).

2.2.6. Colon incision and re-anastomosis surgery

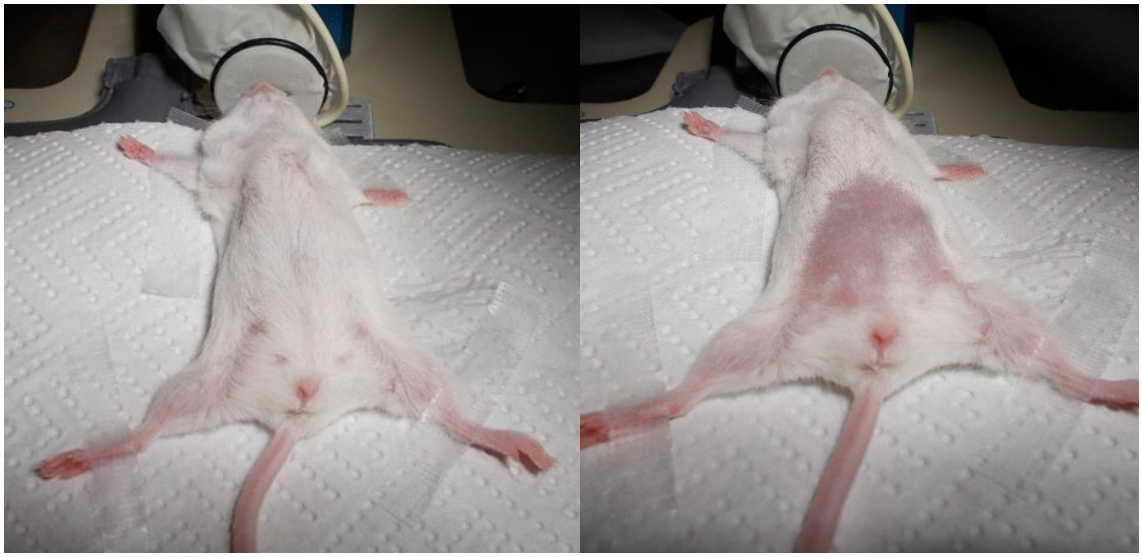

Figure 4: Mouse before surgery.
The animal is fixed under the microscope in a spread-eagled position.
Left: before and right: after shaving and disinfecting the abdomen.
Modified from the supplement of (Miltschitzky, Clees et al. 2021).

The peritoneal cavity was accessed through a median laparotomy of 1.5 to 2 centimeters by dissecting first skin and attached subcutaneous fat with scissors. The peritoneum was incised along the linea alba to preserve abdominal muscle using the same scissors. This approach allowed to minimize bleeding during preparation. A retractor was inserted for good visibility and the operating situs was cleared by mobilizing the small intestine and cecum out of the abdominal cavity. These viscera had to be wrapped into moistened gauze dressings and intermittent irrigation by applying 0.9% sodium chlorine solution into the open abdominal cavity had to be provided during the complete procedure to avoid viscera from drying out and to prevent intraoperative loss of bodily fluid. In addition, about 1 ml of 0.9% sodium chlorine solution was applied intraperitoneally before closing the peritoneum. All contact with any viscera was performed bluntly, using only swabs and anatomic forceps to avoid damaging the fragile tissue. No part of any organ was squeezed or incarcerated at any time during the procedure.

For the delicate microsurgical preparation of the colon, incision and subsequent anastomosis suturing, an operating microscope with 10-fold magnification was used. The rectosigmoidal part of the large intestine was be identified by using the inferior pole of the left kidney as a landmark. First, the mesenterial artery was mobilized and the vessel-free part of the meso in between two branches was pierced using fine pincers to create a hiatus through which one branch of scissors could be inserted to transect the colon injuring any vessels. No part of the colon, meso or the vessels were resected to avoid confounding the experiment with potential ischemic components of anastomotic leakage.

In the rare cases of bleeding, hemostasis was achieved by compression with swabs.

The two separated ends of the intestine were reconnected in an end-to-end anastomosis with 12 single 9-0 Vicryl sutures. First, the anastomosis was anchored with two stitches, one on the mesenterial side of the anastomosis, the other on the antimesenteric side with one end of each fixed with bulldog serrefine clamp. The ventral row of the anastomosis was completed with 5 single, equidistanced stitches. To expose the unfinished half of the anastomosis, the anchors were disengaged so the colon could be flipped around the axis. The dorsal row was completed in the same fashion as the ventral one previously after re-fixing the anchor sutures with serrefines. After trimming the sutures, controlling the situs for any bleeding and anatomical reposition of all viscera into the abdominal cavity peritoneum and skin were closed using a running suture of 5-0 Prolene.

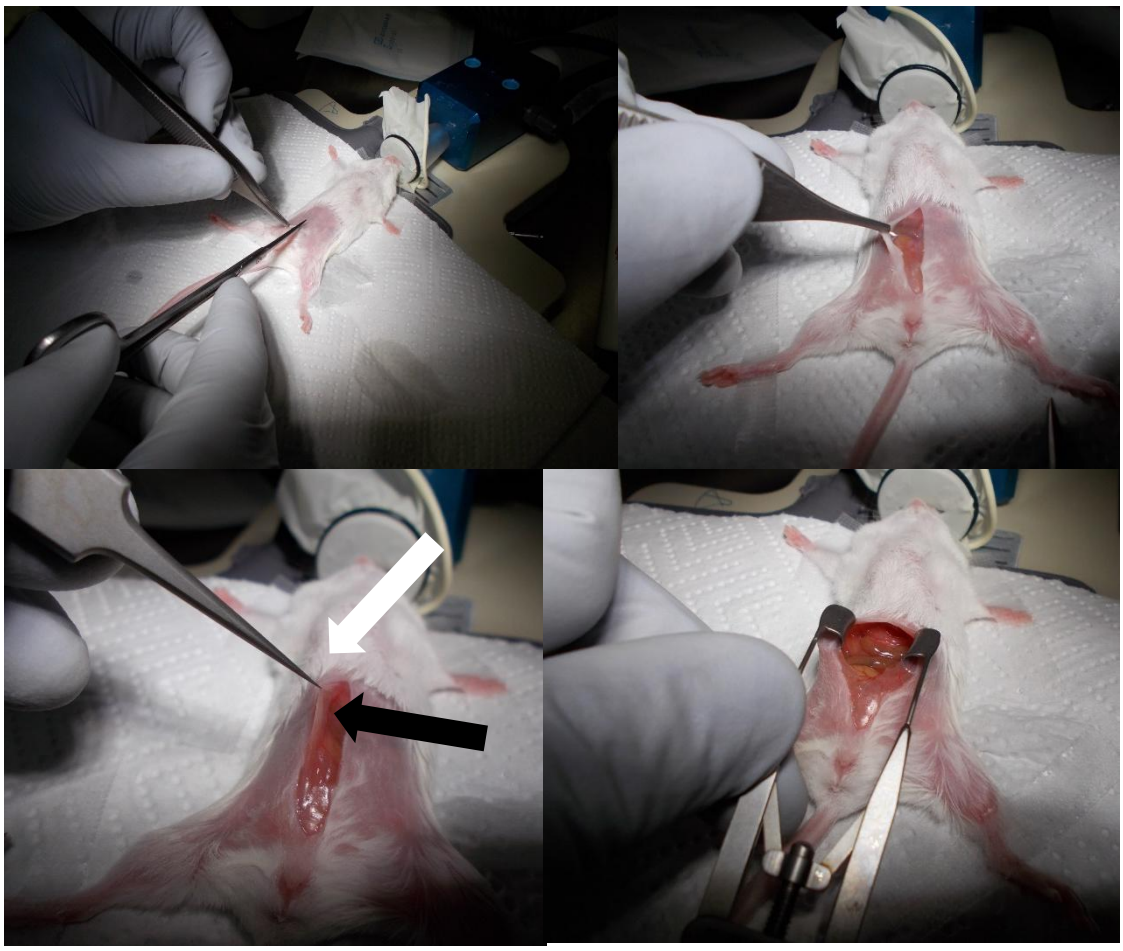

Figure 5: First steps of surgery.
Top left: Incision of the skin and subcutaneous fat. Top right: the peritoneum can be seen through the skin incision.
Bottom left: the linea alba (white arrow, lifted in pincer) needs to be displayed as an identification mark for the incision to avoid injury of the epigastric vessels (left epigastric vessels marked by black arrow) to both sides of said line. Bottom right: inserting the retractor provides the exposure needed.
Modified from the supplement of (Miltschitzky, Clees et al. 2021).

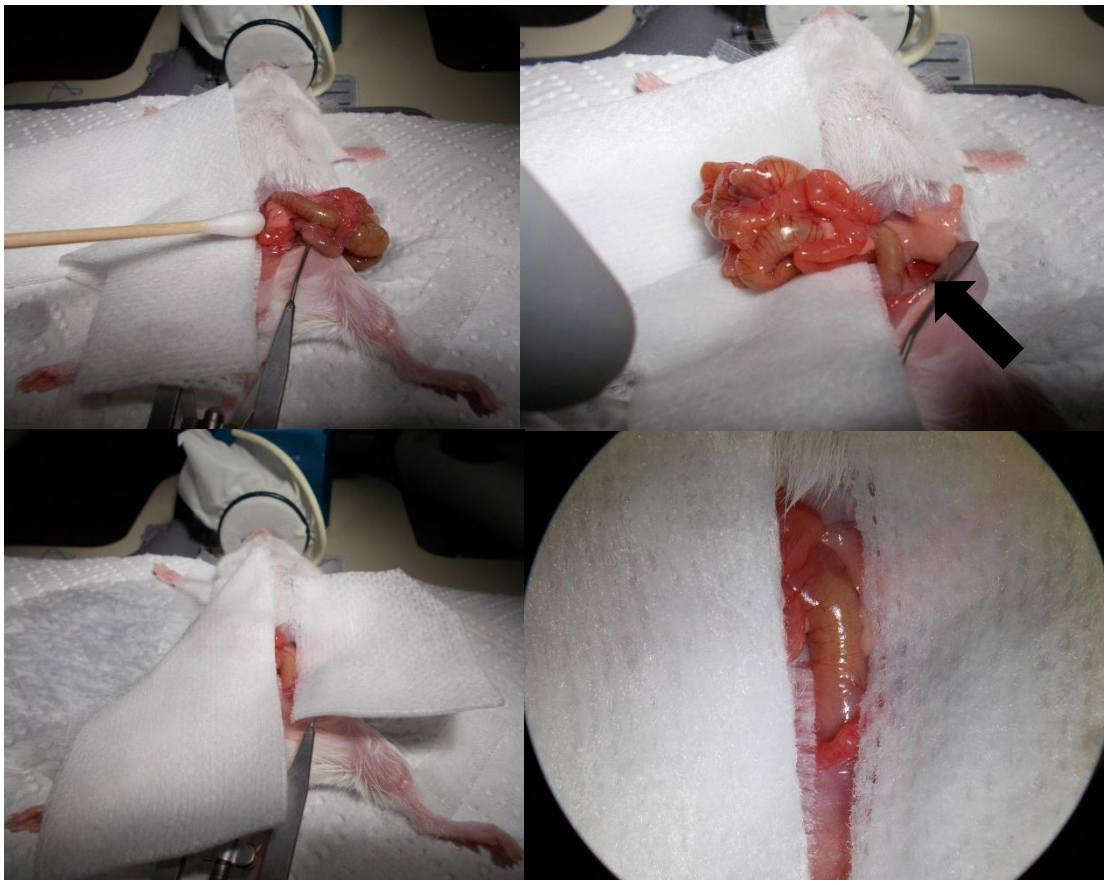

Figure 6: Mobilization of the intestine.
Top left: the small intestine and cecum are first mobilized to the left. Top right: moist gauze dressings are placed onto the right dorsal wall of the abdominal cavity to support and protect the bowels. The bowels are then luxated to the right and wrapped in gauze. Note the position of the lower left kidney pole (black arrow), which serves as orientation for the incision of the colon at the recto-sigmoidal transition later.
Bottom row: after wrapping the luxated bowels and inserting a second sheet of moistened gauze on the left side of the incision, all viscera are covered leaving only the relevant part of the colon exposed.
Top row and bottom left: direct view onto the situs with the surgical lights on. Bottom right: View through the operating microscope.
Modified from the supplement of (Miltschitzky, Clees et al. 2021).

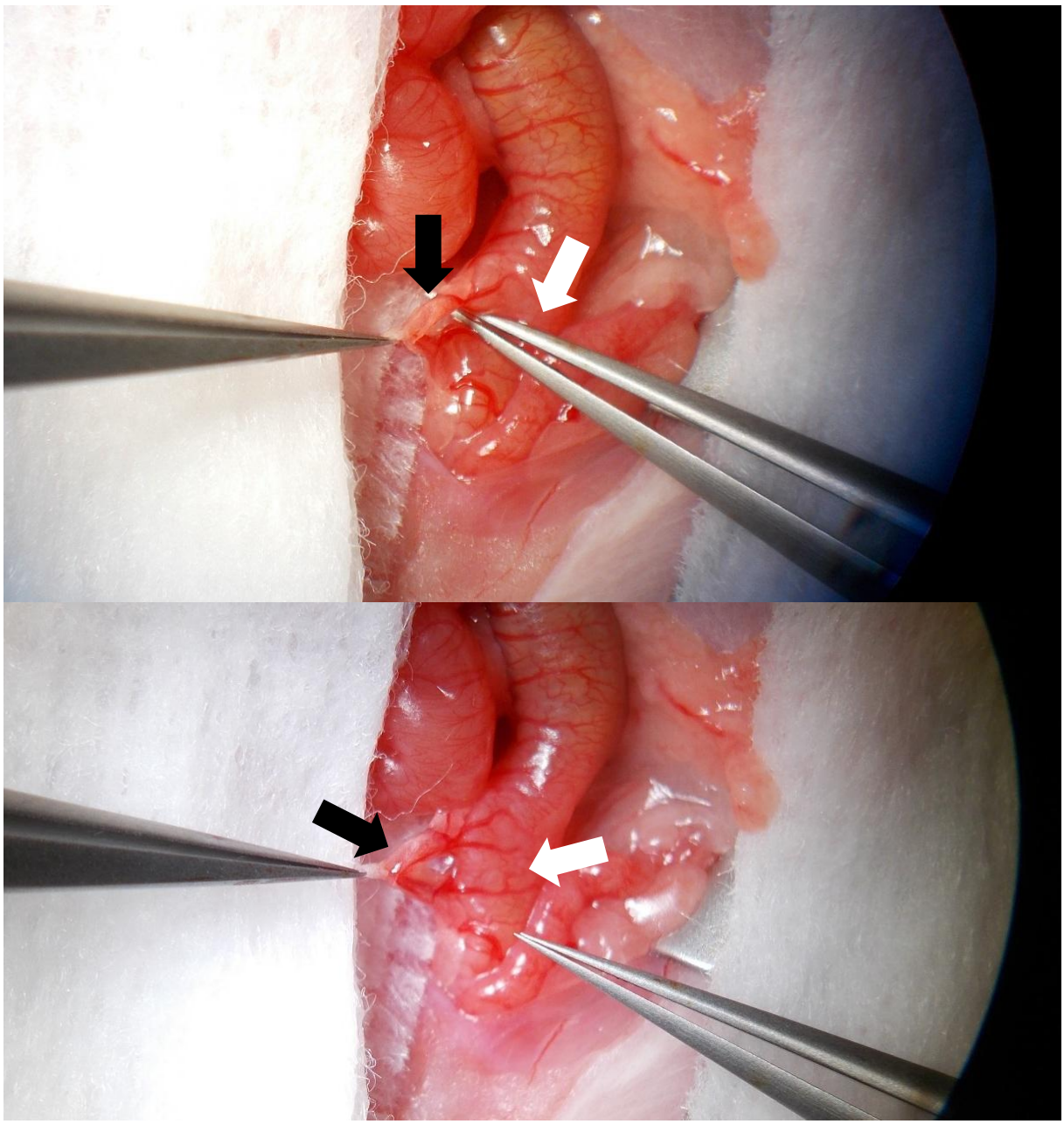

Figure 7: Preparation of the incision site.
View through the operating microscope. Top: A hole can be opened in the membranous part of the meso in between the vessel arcades with one set of fine pincers lifting the meso (top, black arrow) and the other one burrowing (top, white arrow). Bottom: This leaves a gap into in between the meso with the mesenterial artery clearly visible (bottom, black arrow) and the colon (bottom, white arrow), into which the scissors can be inserted for incision later.
Modified from the supplement of (Miltschitzky, Clees et al. 2021).

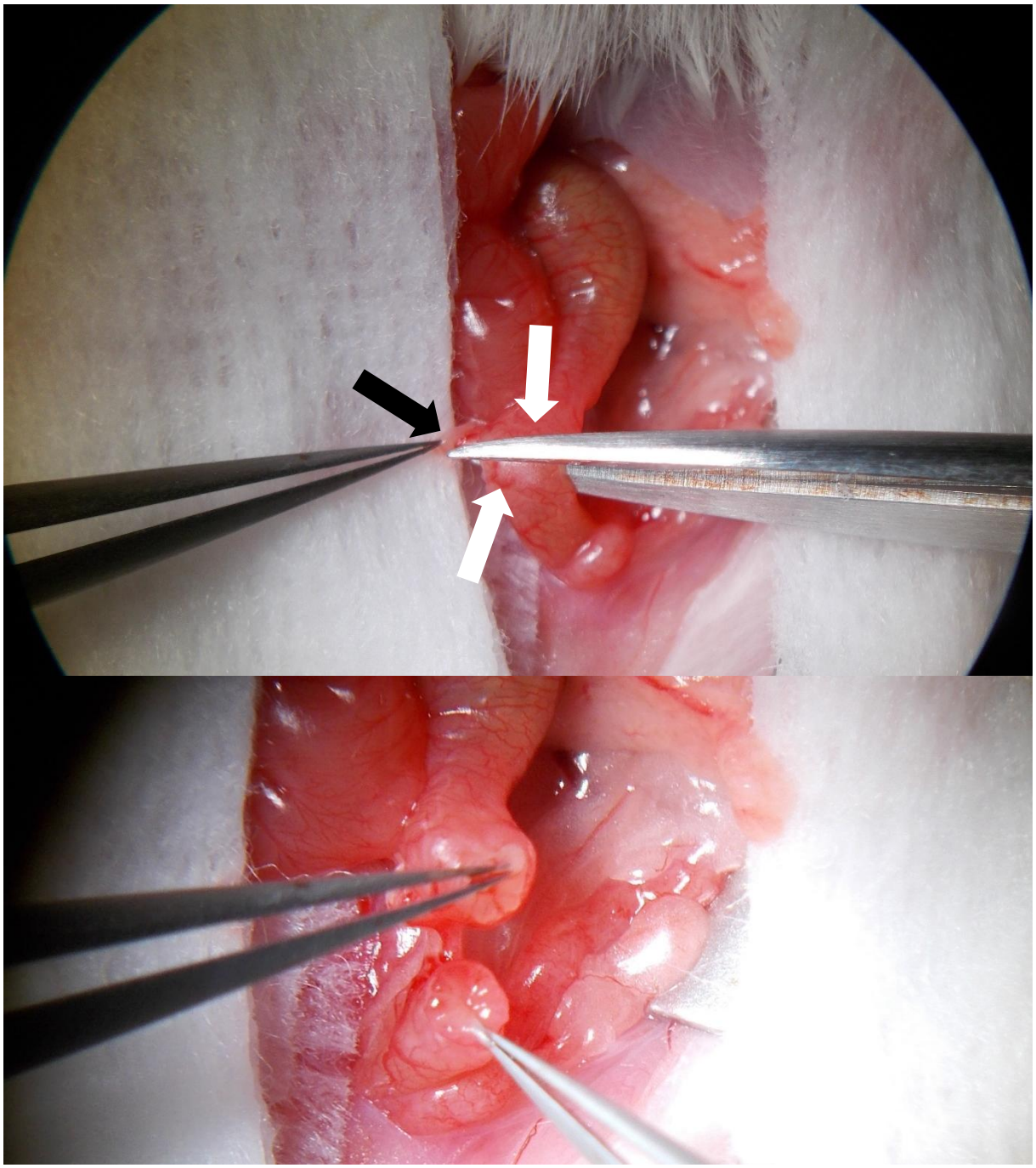

Figure 8: Incision of the colon.
View through the operating microscope. Top: one blade of the scissors is carefully pushed under the colon and through the gap in the meso, ensuring that A) the meso with the mesenterial artery (black arrow) is not caught in between the blades and that B) the incision is parallel to the arcade vessels (white arrows) to avoid any injury to the vessels resulting in bleeding or malperfusion of the tissue. Bottom: After the incision, some contraction of the circular muscle of the colon stumps or even a spasm is normal. Lack of bleeding from the stumps as seen in this photo is the benchmark sign of a clean incision without injury to the vessels.
Modified from the supplement of (Miltschitzky, Clees et al. 2021).

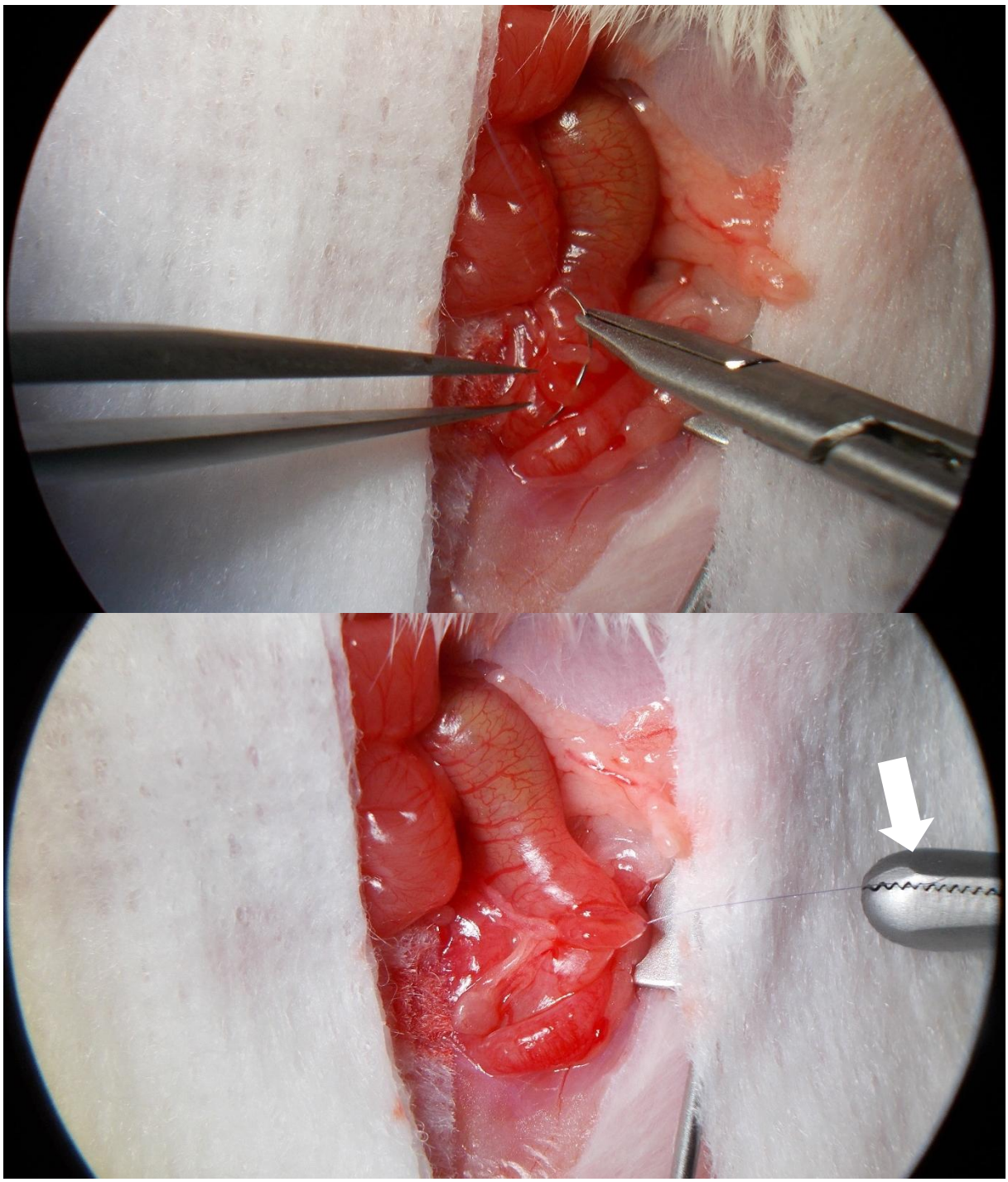

Figure 9: First anchoring suture.
View through the operating microscope. Top: using a fine needle holder and a 9-0 Vicryl suture, the first suture is placed directly opposite the meso. Bottom: after knotting, one suture end is left long and attached to a bulldog serrefine (white arrow).
Modified from the supplement of (Miltschitzky, Clees et al. 2021).

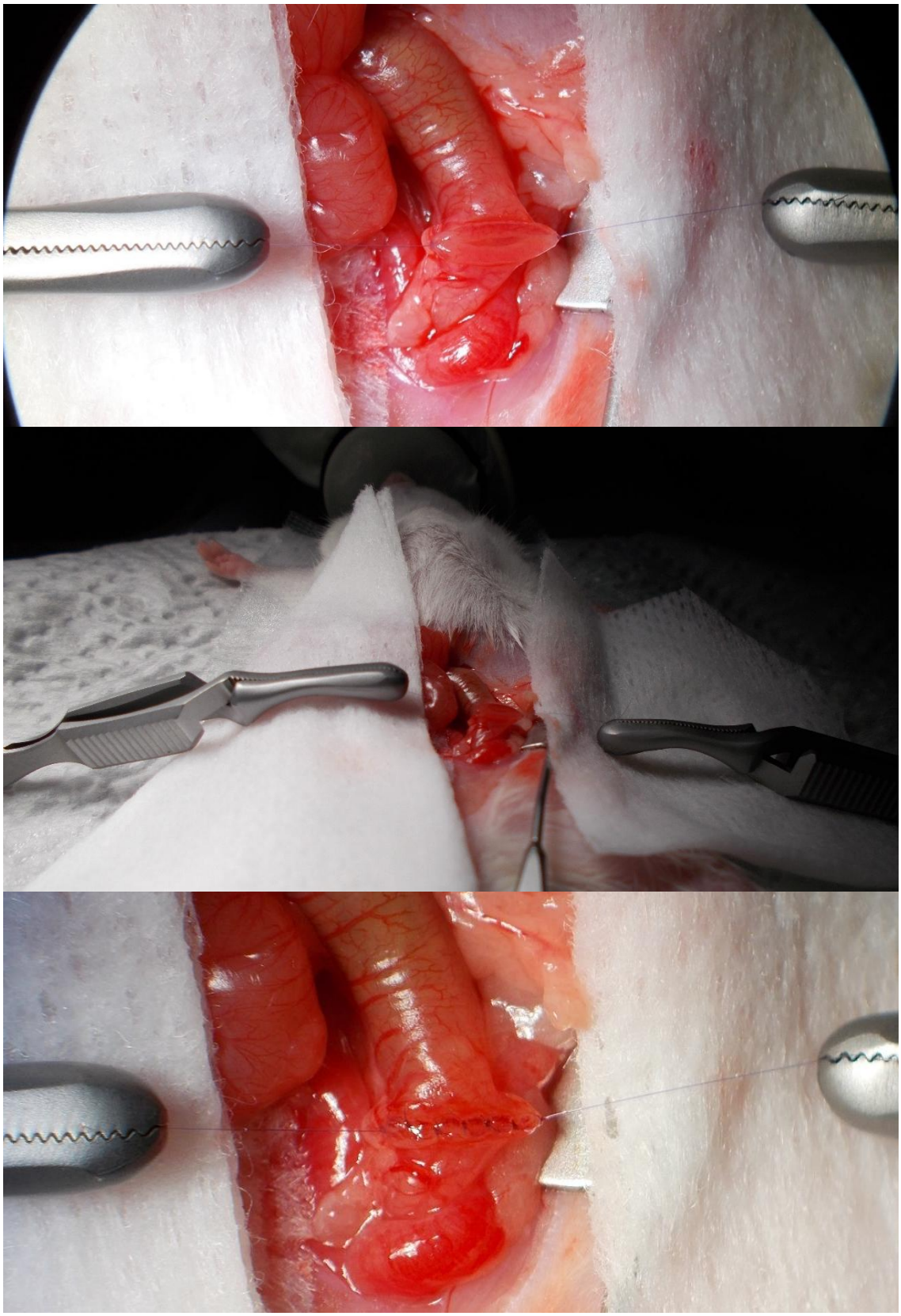

Figure 10: Completion of the ventral row of sutures.
In the same fashion, the second anchoring suture is inserted at the mesenterial side and attached to a bulldog serrefine. Top: view through the operating microscope. Middle: direct view with only ambient lights on. Bottom: By inserting 5 stitches equally spaced in between the two anchors, the ventral row is completed. The tendency of the colonic tissue to form everted "lips" at the site of the anastomosis needs to be counteracted by guiding the needle on a course tangential to the wall of the colon when suturing. View through the operating microscope
Modified from the supplement of (Miltschitzky, Clees et al. 2021).

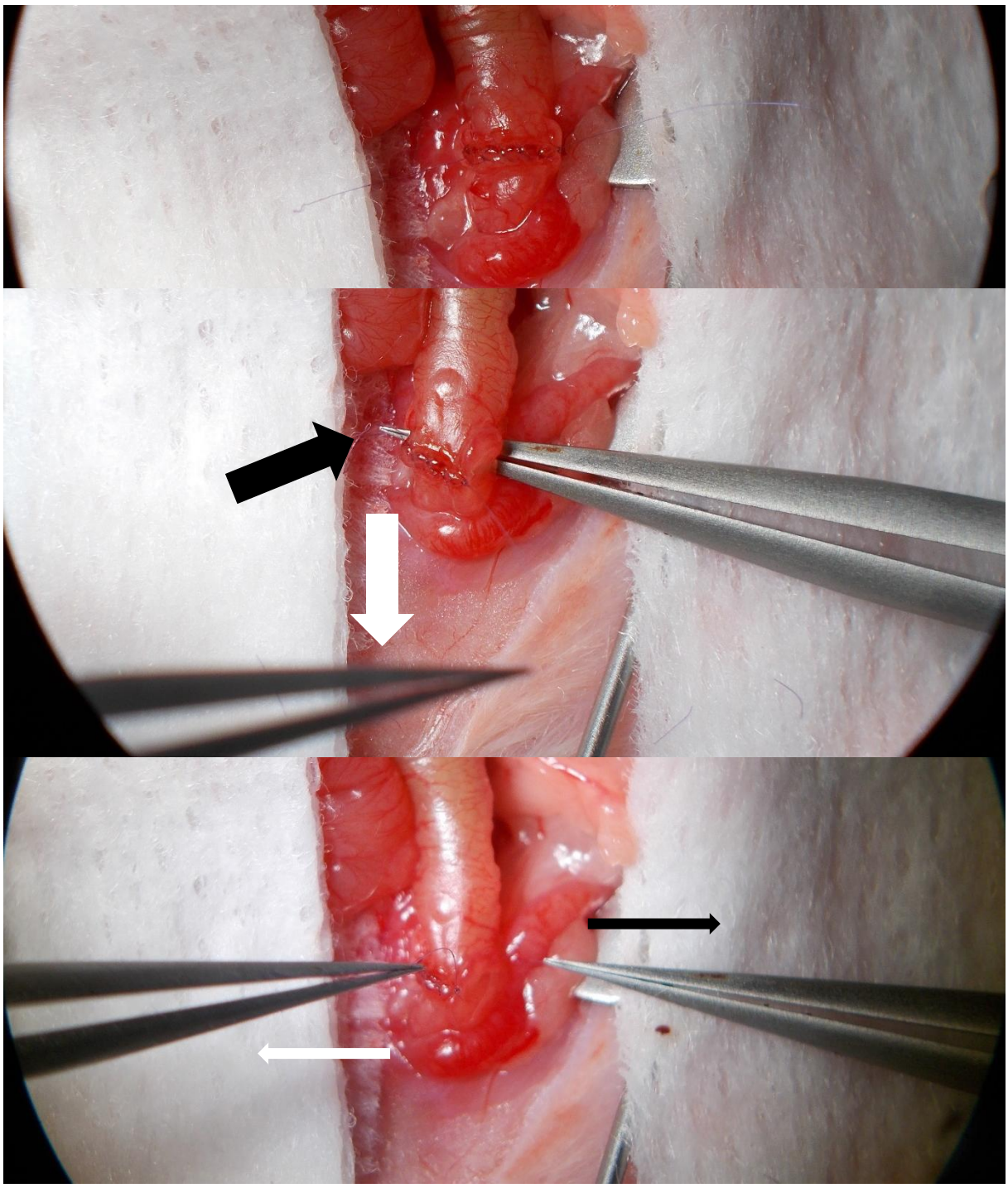

Figure 11: The "flipping maneuver".
Top: After detaching the bulldog serrefine clamps... Middle: ...the colon is lifted by grabbing the anti-mesenterial anchor with fine pincers held in the left hand (white arrow) and inserting the right-hand-set of pincers through the gap in the meso to grab the mesenterial anchor (black arrow). Bottom: After getting hold of the mesenterial anchor, the colon can be flipped over by pulling the mesenterial anchor to the left, through the gap in the meso (direction of the slim black arrow) while the anti-mesenterial anchor is pulled to the right (direction of the slim white arrow), thus exposing the dorsal side of the anastomosis. All views through the operating microscope.
Modified from the supplement of (Miltschitzky, Clees et al. 2021).

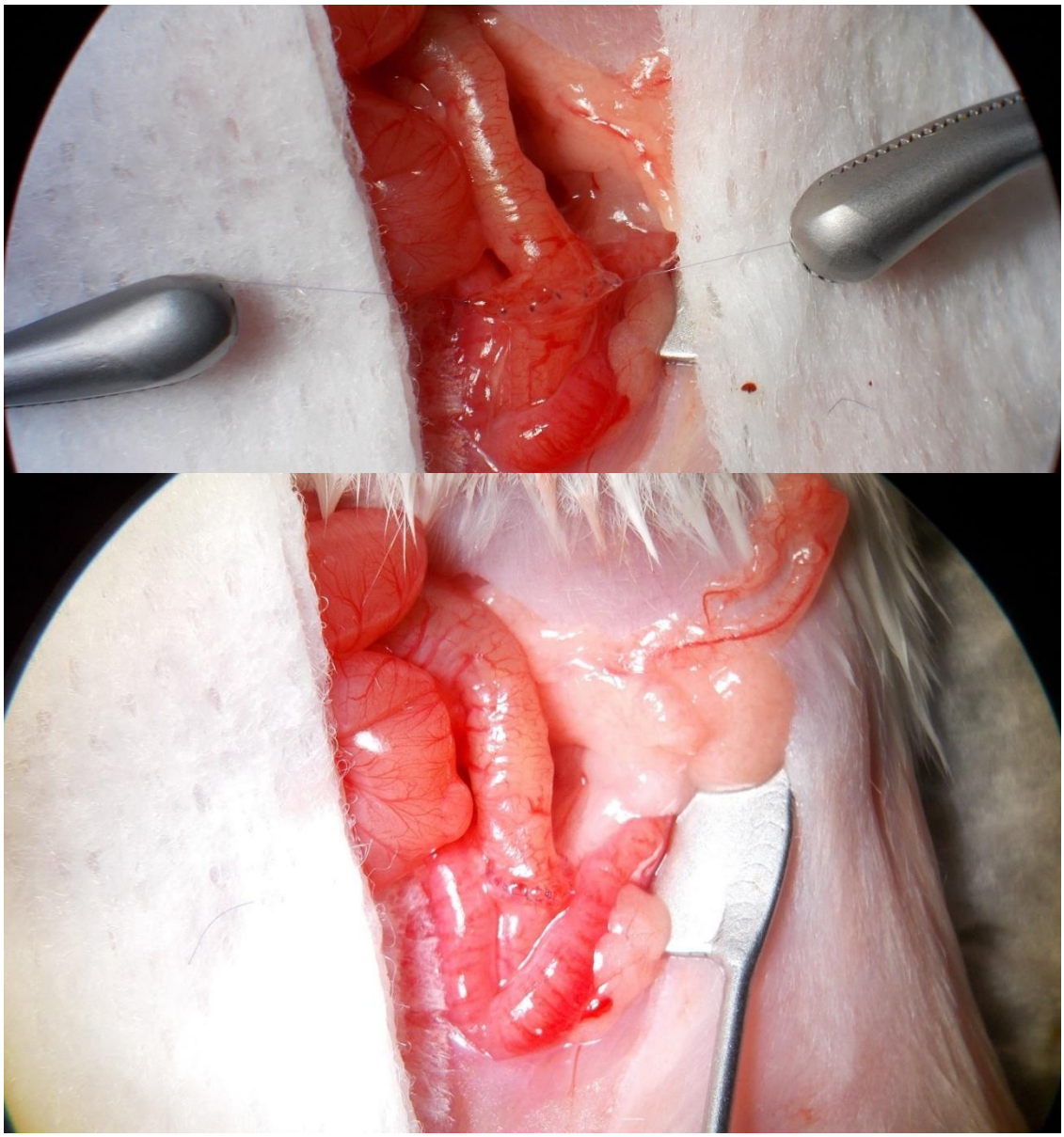

Figure 12: Completion of the anastomosis.
Top: the dorsal row is completed with 5 stitches like the ventral one, adding up to a total of 12 stitches. If the perfect spacing cannot be achieved, the number of stitches can be adapted to a number between 10 and 14 stitches as needed to provide regular spacing. Bottom: finished anastomosis after shortening the two anchor sutures to normal length. Views through the operating microscope.
Modified from the supplement of (Miltschitzky, Clees et al. 2021).

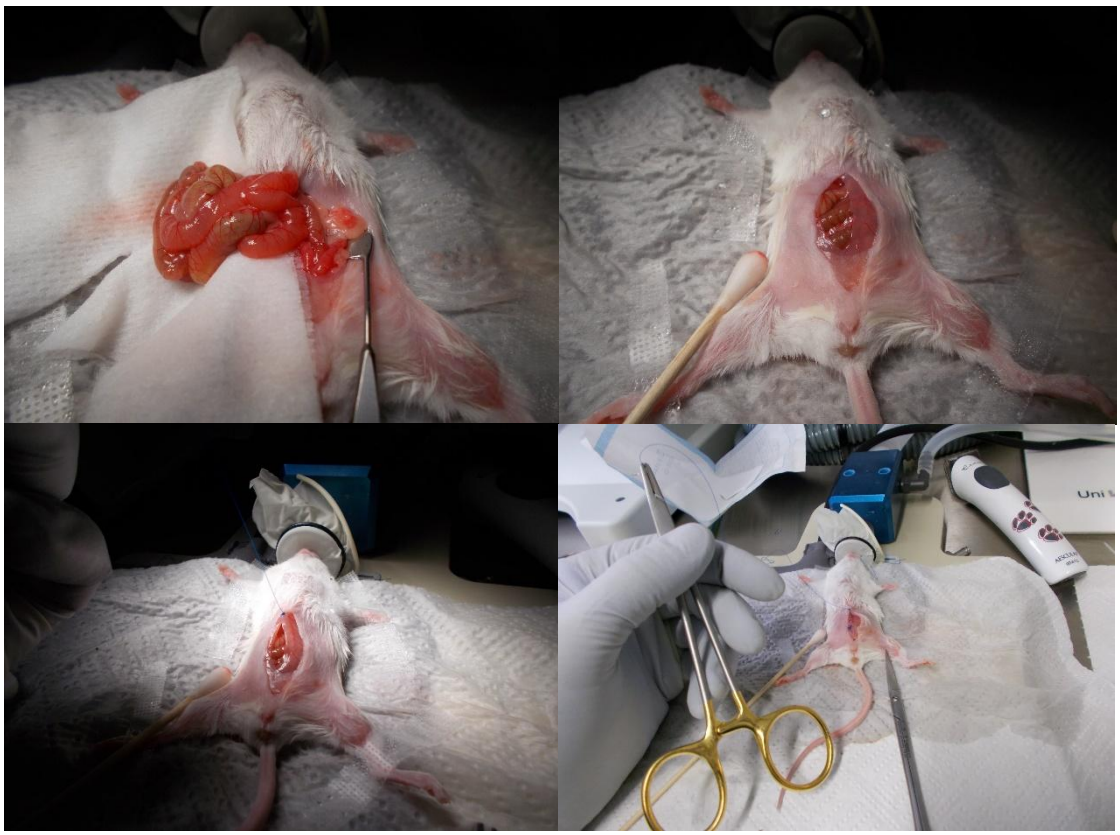

Figure 13: Final steps of surgery.
Top left: unwrapping... Top right: ...and blunt reposition of the luxated viscera. Direct views with only ambient lights on. Bottom left: After repositioning the viscera, the peritoneum is closed with a running suture. Direct view after the first stitch under surgical lights. Bottom right: After closure of the peritoneum, the skin is closed in a running stitch suture using 5-0 Vicryl. Direct view under ambient lights.
Modified from the supplement of (Miltschitzky, Clees et al. 2021).

2.2.7. Finalization of the experiment

2.2.7.1. Sacrificing mice

All experiments were finalized by cervical dislocation under general anesthesia (see 2.2.4). The mouse's *os occipitale* was fixated against a hard surface using coarse pincers. The cervical spine was then dislocated by pulling the tail firmly. Instant death occurred and was ascertained by palpation of the discontinuity of the cervical spine.

2.2.7.2. "Swiss roll"

The colon is cut open lengthwise and rolled into a spiral (which we have dubbed "Swiss roll"), then fixated in formalin, embedded in paraffine, cut and stained with H&E. The slides of the Swiss roll are then scanned into a high-resolution digital slide (*.MRXS file).

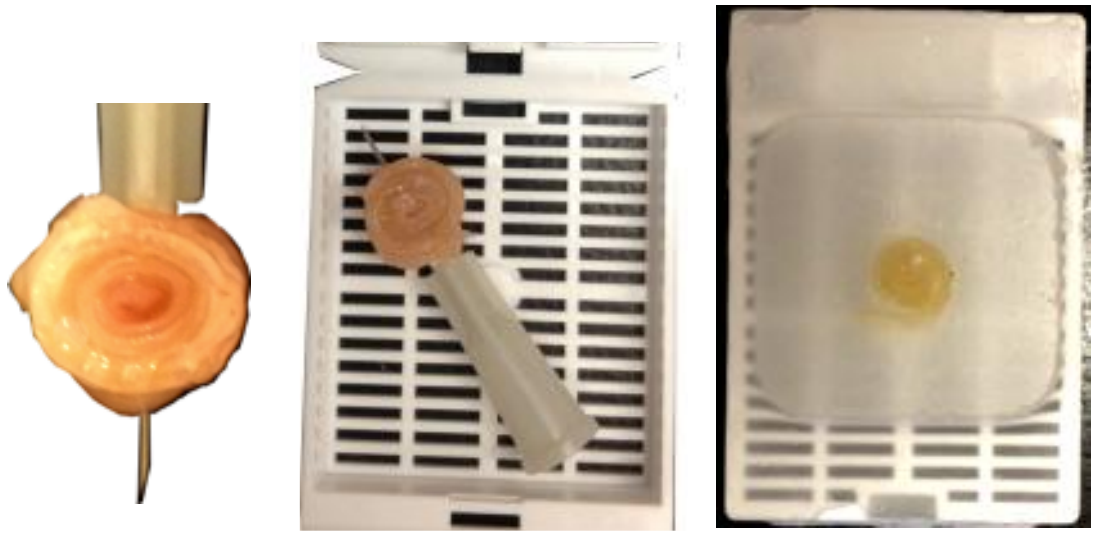

Figure 14: Embedding of a Swiss roll in paraffine.
P.-A. Neumann, 2016, previously unpublished, with friendly approval of the author.

2.2.7.3. Tissue extraction of anastomosis samples

After longitudinal laparotomy in the dead animal, the anastomosis was mobilized, all adhesions were removed, taking notes for the adhesion score (see 2.2.8.2) and the part of the intestine containing the anastomosis was taken out for further analysis.

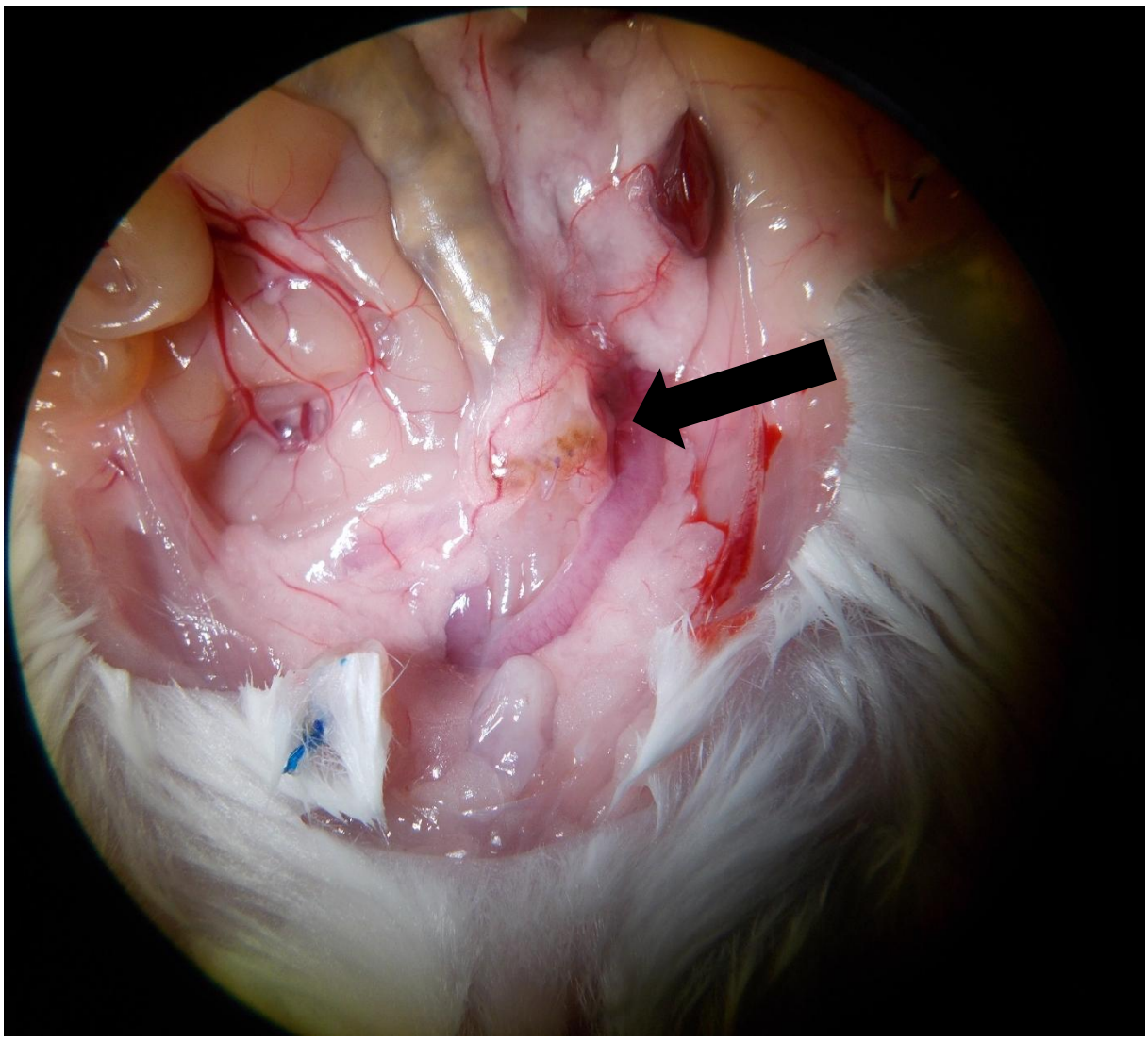

Figure 15: Anastomosis in situ on POD7.
The anastomosis (black arrow) is covered by adherent omentum and uterus.
View through the operating microscope.
Own photography, previously unpublished.

2.2.7.3.1. Bursting pressure measurement

Modified from (Miltschitzky, Clees et al. 2021).

After extracting the colon and clearing it of feces with a swab (see 2.2.7.3.2), the colon was mounted onto a petri dish with a i.v. feed inserted into the lumen on the aboral side of the anastomosis and a pressure-probe on the oral side. Both sides were fixed to the probes with 4-0 sutures (see Figure 16). After calibrating the pressure to 0 mmHg, the colon was filled with 0.9% sodium chlorine solution until bursting under constant measurement of intraluminal pressure. Then the maximum of the pressure spike and the location of the burst were noted.

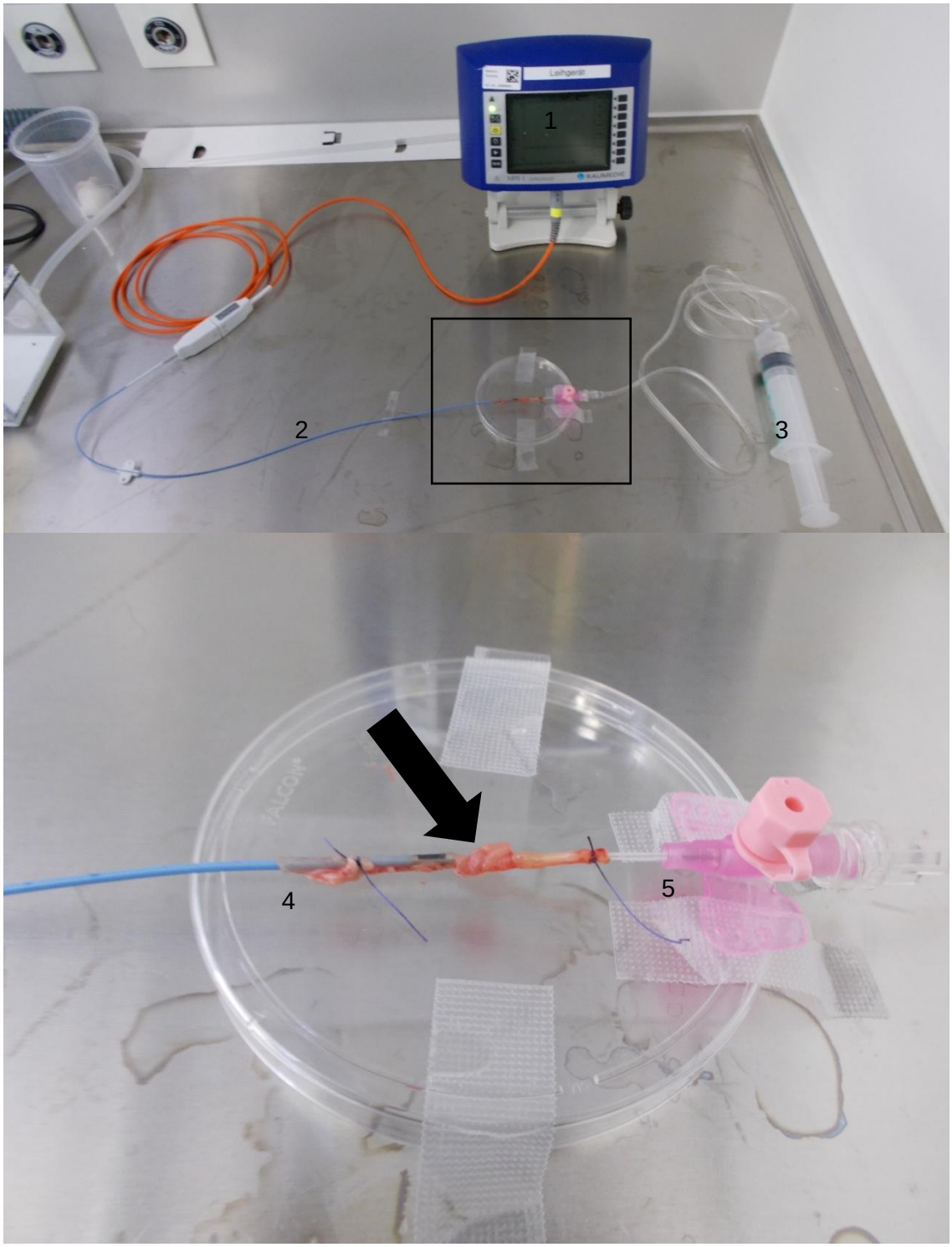

Figure 16: Bursting pressure measurement setup.
Top: overview, Bottom: detail marked in the overview.
Mount the colon onto a petri dish with a plastic cannula inserted into the lumen on the aboral side of the anastomosis and an ICP probe on the oral side Both sides are fixed to the probes with 4-0 sutures. After calibrating the pressure to 0 mmHg, the colon is filled with 0.9% sodium chlorine solution until bursting under constant measurement of pressure inside the lumen Then the maximum of the pressure spike is noted as the bursting pressure.1) pressure monitor, 2) ICP probe, 3) syringe, infusion tube and plastic cannula, 4) ICP probe inserted into the part of the colon on the oral side, 5) cannula inserted into the part of the colon on the aboral side of the anastomosis (black arrow).
Modified from the supplement of (Miltschitzky, Clees et al. 2021).

2.2.7.3.2. Sample preparation

Modified from (Miltschitzky, Clees et al. 2021).

Feces was expressed from the colon without disrupting it‘s integrity by gently rolling a swab over it. The fecal matter was sampled for future microbiological analysis. The colon was incised lengthwise along the mesocolon, flattened onto a petri dish, and cut into two halves using a scalpel. One half of the colon sample was immersed in PFA for histo-pathological analysis. From the other half, two samples were taken using a biopsy punch, one containing the anastomosis, the other far from the anastomosis. These were frozen for later mRNA analysis (Miltschitzky, Clees et al. 2021).

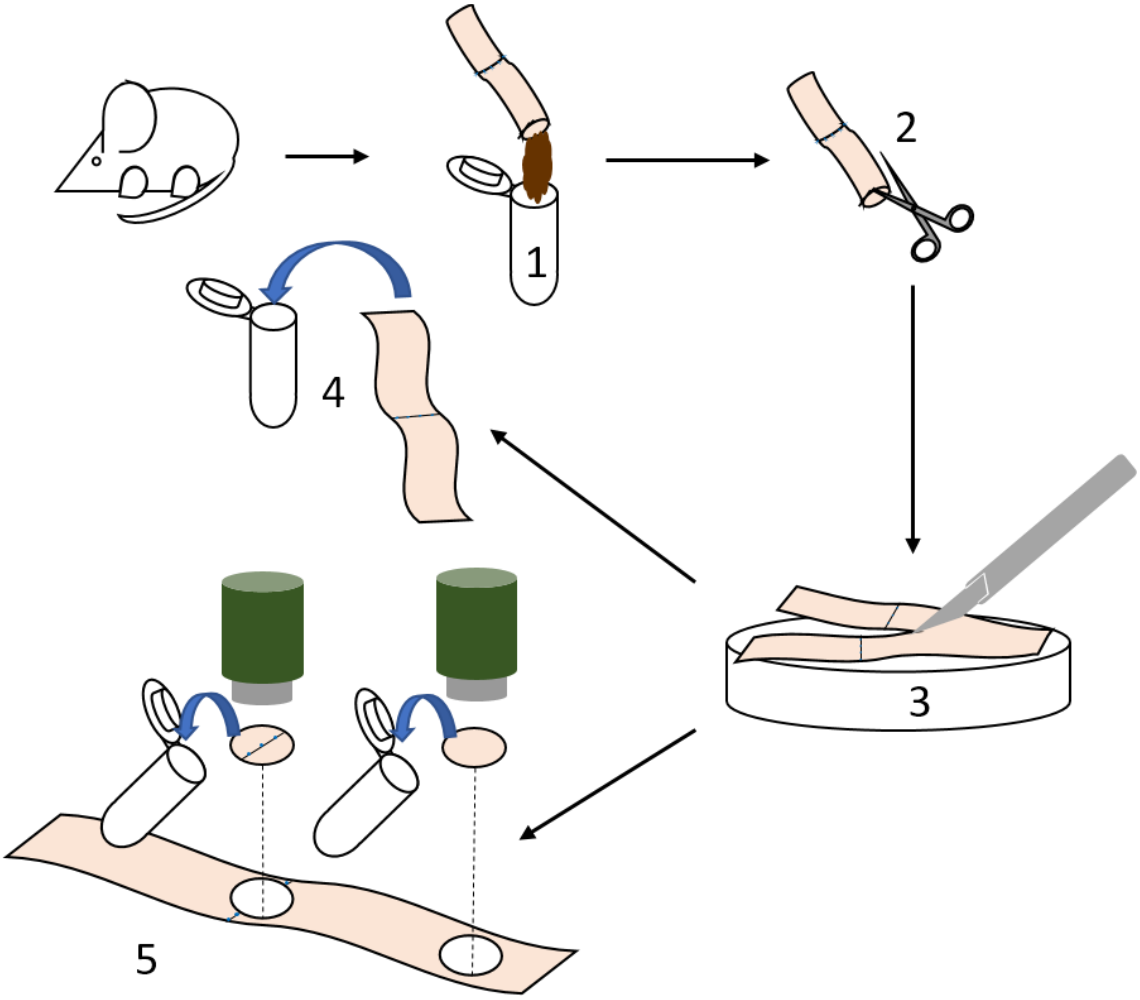

Figure 17: Schematic of sample preparation.
1) feces are collected for microbiological analysis. 2) the colon is dissected lengthwise and 3) spread out onto a petri dish, where it is dissected lengthwise again. 4) One half of the colon is stored in toto, whereas 5) biopsies containing a defined volume of colon tissue are taken from the site of the anastomosis and the colon away from the site of anastomosis.
Figure 5 from (Miltschitzky, Clees et al. 2021)

2.2.8. Scores

2.2.8.1. Disease activity index (DAI)

Modified from (Miltschitzky, Clees et al. 2021).

The disease activity index (DAI) is a widely used scoring tool to clinically assess the health of mice with experimental colitis. With small variations between different publications, it is calculated as follows:

Criteria	**Score points**
Weight loss	0 = none 1 = 1 to < 5% 2 = 5 to < 10% 3 = 10 to < 15% 4 = > 15%
Stool consistency	0 = normal, formed stools 2 = soft, unformed stools 4 = watery diarrhea
Hematochezia	0 = none, negative Hemoccult® 2 = micro-hematochezia, positive Hemoccult® 4 = macroscopically visible blood in stool

Table 3: Calculation criteria of DAI

Adapted Table 1 from (Gonçalves, Schneider et al. 2013)

The points of every category are added, then the result is divided by 3 to yield the DAI:

$$DAI = \frac{\sum Points}{3}$$

2.2.8.2. Adhesion score

Modified from (Miltschitzky, Clees et al. 2021).

The adhesion score awards points for adhesions in different categories. All points are summed up to give the score (0 to 7), higher scores reflect a higher number of adhesions:

Criteria	**Score points**
Are uterus, small intestine or omentum attached to the anastomosis?	1 Point per adherent organ
Is any other organ attached to the anastomosis?	0 = No 1 = Yes

Feasibility of removing the adhesions bluntly with a swab	0 = No adhesions in the first place 1 = All adhesions can be removed bluntly 2 = Only part of the adhesions can be removed bluntly 3 = No adhesions can be removed bluntly at all

Table 4: Calculation criteria of adhesion score
Table 4 from (Miltschitzky, Clees et al. 2021)

In the process of publication of our methods paper, but after completion of the experiments considered in this thesis, we have recognized the need to also consider abscess formation and have thus expanded this score with categories for abscess formation in analogy to the clinical subclasses of stage II diverticulitis in the Classification of Diverticular Disease (Miltschitzky, Clees et al. 2021).

2.2.8.3. Endoscopic healing score

Modified from (Miltschitzky, Clees et al. 2021).

Macroscopic mucosal healing of the anastomosis can be scored using endoscopy *in vivo* (see 2.2.5). The relevant criterium is the degree of dehiscence:

Score points	**Criteria**
0	no dehiscence
1	suture thread protruding into lumen
2	slight dehiscence, necrotic tissue, or fibrin on less than a quarter of circumference
3	advanced dehiscence, necrotic tissue, or fibrin on more than a quarter of circumference
4	full dehiscence, visible hole into the peritoneal cavity

Table 5: Calculation criteria for the endoscopic healing score
Table 2 from (Miltschitzky, Clees et al. 2021)

2.2.8.4. Histological colitis score

During induction of experimental DSS colitis, the extent of intestinal inflammation is generally evaluated using a clinical disease activity index (DAI, see 2.2.8.1). Although the DAI produces somewhat variable results depending on user experience, it is generally robust enough to provide reliable information on the experiment in progress and is thus widely used by IBD researchers.

In contrast, there is no generally accepted method for histological evaluation of mucosal damage at the study endpoint. Most commonly, selected areas of the colon are inspected by a trained pathologist and scored based on several parameters that usually include crypt erosion and leukocyte infiltration. However, because the number of investigated parameters and the amount of tissue included in the analysis vary considerably between

individual reports, the comparability of many published studies is limited. To reduce observer bias and enhance interstudy comparability, an ideal histological scoring protocol should:

1. not pick small areas for presentation but include the entire length of the colon, as intestinal inflammation can often present with skip lesions (see Figure 18)

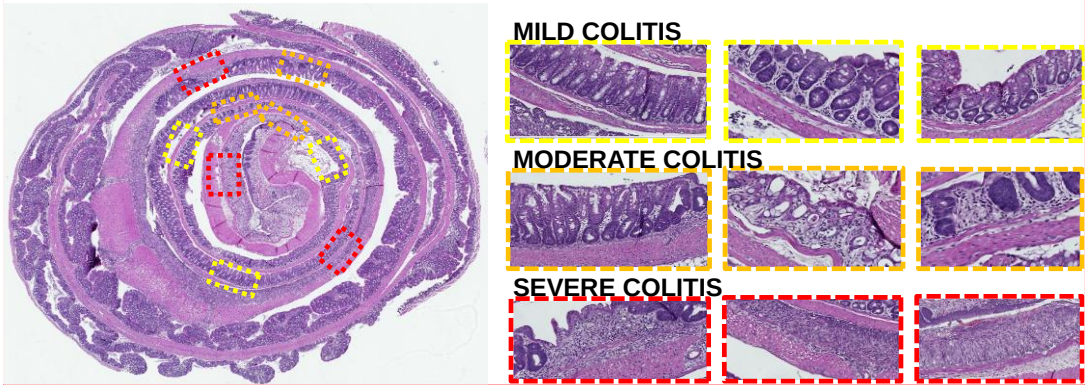

Figure 18: Scanned Swiss roll slide.
Within one animal a wide range of regions with different severity of colitis-associated histological changes from mild (yellow), moderate (orange) to severe colitis (red) can be found. Analysis of the entire colonic mucosa is needed for accurate analysis.
P.-A. Neumann, 2016, previously unpublished, with friendly approval of the author.

2. limit analysis to few, easily interpretable parameters to reduce subjectivity and required expertise.
3. be simple enough to facilitate fast, consistent processing of large sample volumes, and use widely available, affordable tools for data acquisition, analysis, and presentation.

We have developed such a scoring system for analyzing intestinal inflammation and mucosal damage in the DSS using scanned “Swiss rolls” (see 2.2.7.2).

The score is based on three categories of parts of mucosa: healthy, injured and ulcerated. Injured mucosa is characterized by abnormal crypt architecture, submucosal edema or infiltration of leucocytes. Ulcerated parts are denuded of crypts altogether.

The length of the total, injured, and ulcerated mucosa was determined by drawing manual annotations in Aperio ImageScope software along the *muscularis mucosae* layer and reading out the length of the annotations.

Then the histological colitis score can be calculated:

$$HCS = 10 * \frac{injured\ lenght + 2 * ulcerated\ lenght}{total\ length} = \frac{\%injured + 2 * \%ulcerated}{10}$$

This formula considers that ulceration is a sign of graver disease than simple injury by weighting the ulcerated parts doubly.

2.2.8.5. Histopathological score

Modified from (Miltschitzky, Clees et al. 2021).

Histopathological scoring of the anastomosis is one of the most objective and exact measures to evaluate the healing process. Here performance of the microscopic sections and correct alignment of the anastomosis is pivotal.

Criteria	**Score points (maximum = 29)**
Blood vessel ingrowth	0 = no evidence 1 = occasional evidence 2 = light scattering 3 = abundant evidence 4 = confluent cells or fibers
Fibroblasts	0 = no evidence 1 = occasional evidence 2 = light scattering 3 = abundant evidence 4 = confluent cells or fibers
Collagen formation	0 = no evidence 1 = occasional evidence 2 = light scattering 3 = abundant evidence 4 = confluent cells or fibers
Inflammatory cells	0 = confluent cells or fibers 1 = abundant evidence 2 = light scattering 3 = occasional evidence 4 = no evidence
First layer in which continuity has been restored (counted from the mucosa outwards towards serosa)	0 = no layer restored 1 = serosa 2 = muscularis 3 = submucosa 4 = mucosa
Number of healed layers	0 – 4 (none, mucosa, submucosa, serosa)
Epithelium closed	0 = no 1 = yes
Crypt architecture restored	0 = no 1 = yes
Overall healing quality	1 = bad 2 = normal 3 = good

Table 6: Scoring points for the histological healing score.
Table 3 from (Miltschitzky, Clees et al. 2021)

The H&E-stained samples of all anastomoses have been scored in a blinded fashion. The score points in all categories were summed up. Higher scores indicate more advanced healing.

3. Results

3.1. DSS Dose-finding

The timeframe and dose for the surgical experiments had to be chosen to ensure an inflamed, but not completely ulcerated mucosa which we estimated should result in a target histological colitis score of 2-3. In our preliminary dose-finding experiments (groups D2 through D5, see 2.2.1) this did not correlate with the DAI (see 2.2.8.1 and Figure 19. Pearsons r= -0.78 with a 95% CI [-0.99 to 0.32], *p=0.12* for 2% DSS, 0.73 [-0.06 to 0.96], *p=0.06* for 3% DSS and 0.69 [-0.28 to 0.96], *p=0.13* for 5% DSS).

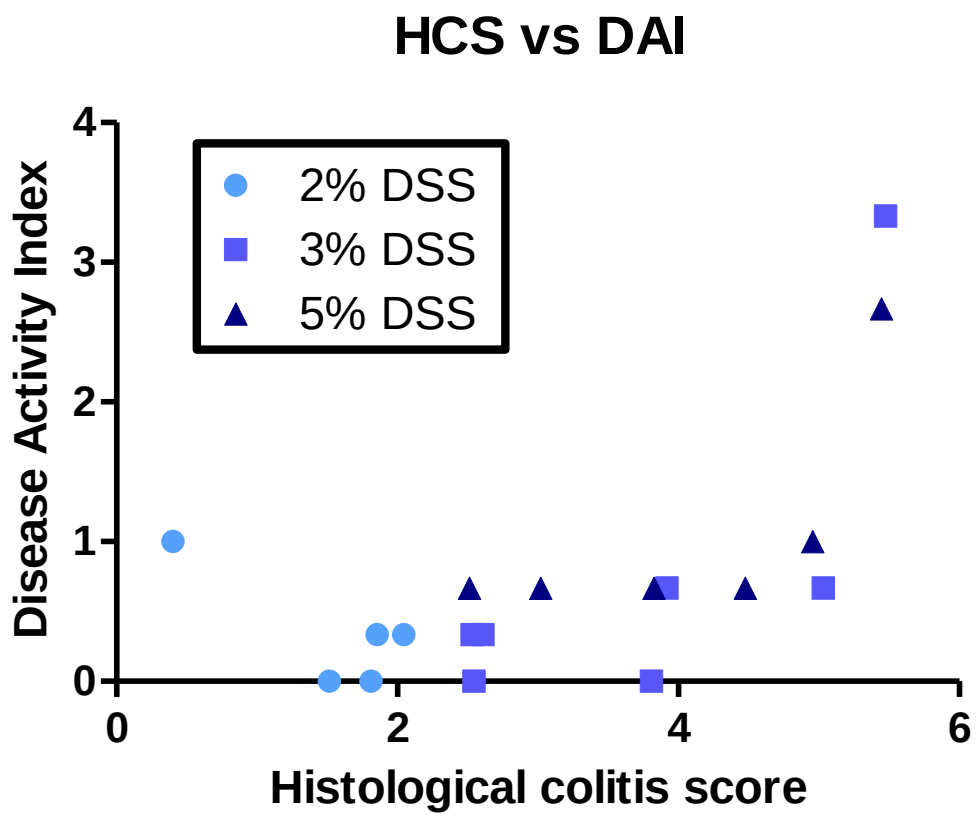

Figure 19: Scatterplot comparing histological colitis score and DAI.
Own figure based on experimental data.

As to mere weight loss, the D2-group gained an average 1.03% (95%-CI: [-3.78%; 1.71%]) of weight during induction, the D3 group gained 0.62% (95%-CI: [-2.68%; 1.43%]), whereas the D5 group lost an average of 5.60% (95%-CI: [3.99%; 7.21%]) of weight. In short, only 5% of DSS yielded any significant loss of weight after 7 days of exposure. We therefore started the D0 group on 5% of DSS during induction, followed by surgery.

3.2. Aborted D0 group

The D0 group was started on an induction with 5% of DSS for 7 days, followed by surgery. Of the 14 animals operated until the experiment with this group was halted, only 3 successfully reached their respective endpoint. It is noteworthy, that for two of these, that was POD3. Only one mouse reached POD7 as planned. 5 of the unsuccessful animals were found dead, 2 on POD1, 3 on POD2. The other 6 animals had reached the aborting criteria specified in 2.2.2. Two of these developed suture dehiscence, 4 excessive weight loss, in 3 cases of more than 20%. It is notable, that in the two successful animals evaluated on POD3, there was a complication during surgery: in one case 2 stitches of the anastomosis were torn out and had to be revised during the procedure and in one case there was slight bleeding from the incised colon. There was bleeding in 4 of the unsuccessful cases and a torn stitch in one.

Analysis of the reasons for this failure led to the decision to continue the surgery experiments with 2% of DSS. Due to the small number of animals (i.e., 3) which reached their respective endpoints, the data from the evaluation of these was not considered for the analysis in 3.3.

3.3. The effect of Ac2-26-loaded nanoparticles on anastomotic healing (H0, DX, DS and DA groups)

3.3.1. Weight loss and recovery

The arithmetic mean of the weight relative to the initial measurement with 95% confidence intervals is shown in Figure 20 for H0- (surgery, no colitis, no treatment), DX- (DSS colitis, surgery, no treatment), DS- (DSS colitis, surgery, sham treatment with i.p. injections of Scrm-NP) and DA-group (DSS colitis, surgery, treatment by i.p. injections of Ac2-26-NP) with evaluation on POD3, Figure 21 for groups with evaluation on POD7 and Figure 22 for groups with evaluation on POD14.

The baseline for the relative weight is the initial measurement before surgery for H0 groups, the measurement before the start of the DSS-colitis induction phase for DX, DS and DA groups. For the DS group, only DS-03 and DS-07 subgroup experiments and no DS-14 experiment were conducted (see 2.2.1).

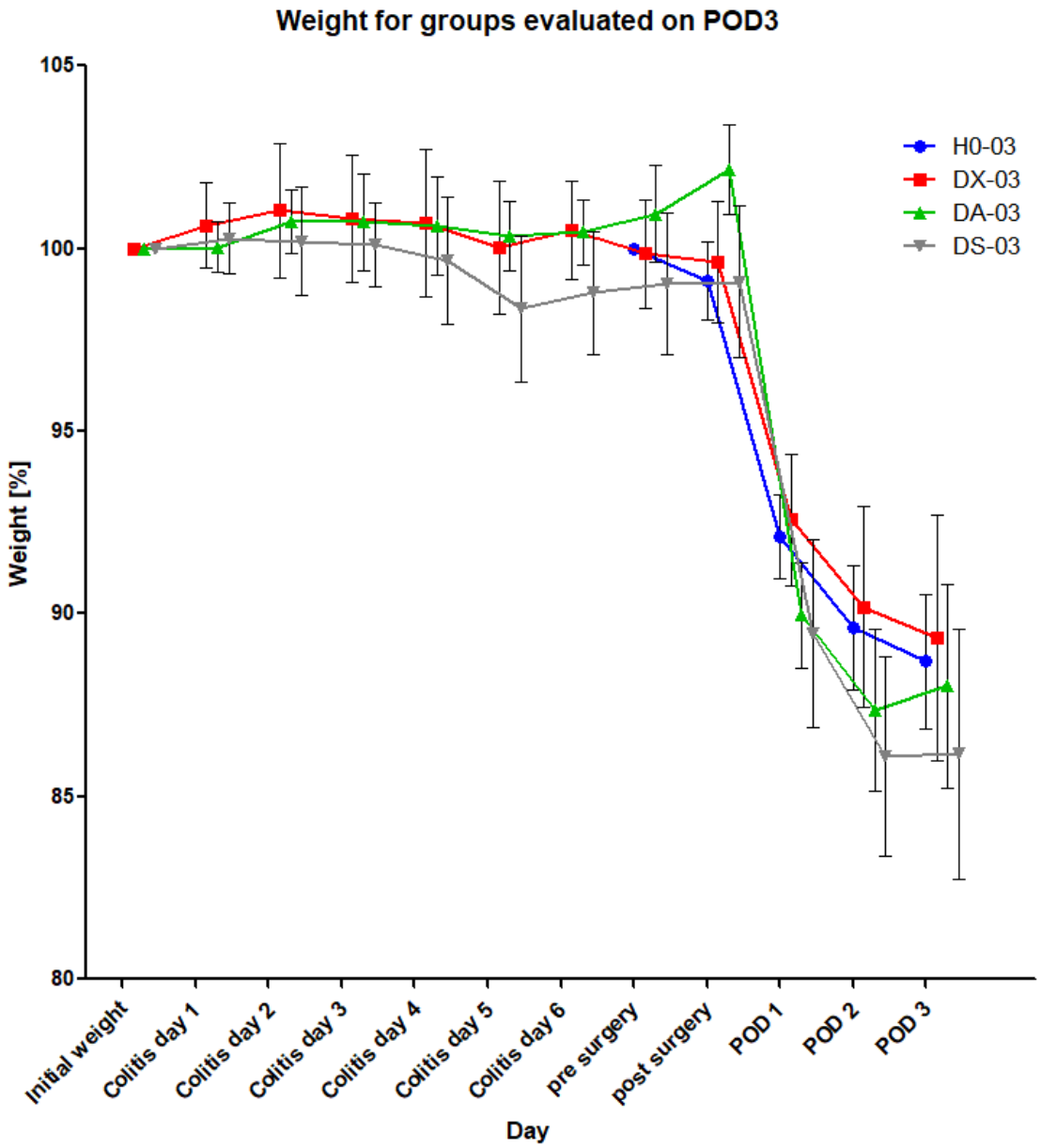

Figure 20: Mean weight curves for H0, DX, DA and DS groups evaluated on POD3.

Group designations: H0: water control group; surgery without DSS-colitis or treatment. DX: DSS-control group; DSS-colitis with 2%, surgery, no treatment. DS: scramble-control group; DSS-colitis with 2%, surgery, sham treatment with Scrm-NPs. DA: experiment group; DSS-colitis with 2%, surgery, treatment with Ac2-26 NPs.

The bars signify the 95% confidence interval. Note that no weight measurements have been taken for the H0 group until the preoperative measurement, since there is no colitis induction phase. The weight of the animals in the colitis groups is distributed around 100% of the initial weight during induction of DSS colitis, followed by a distinct drop of 10-15% after surgery.
Own figure based on experimental data.

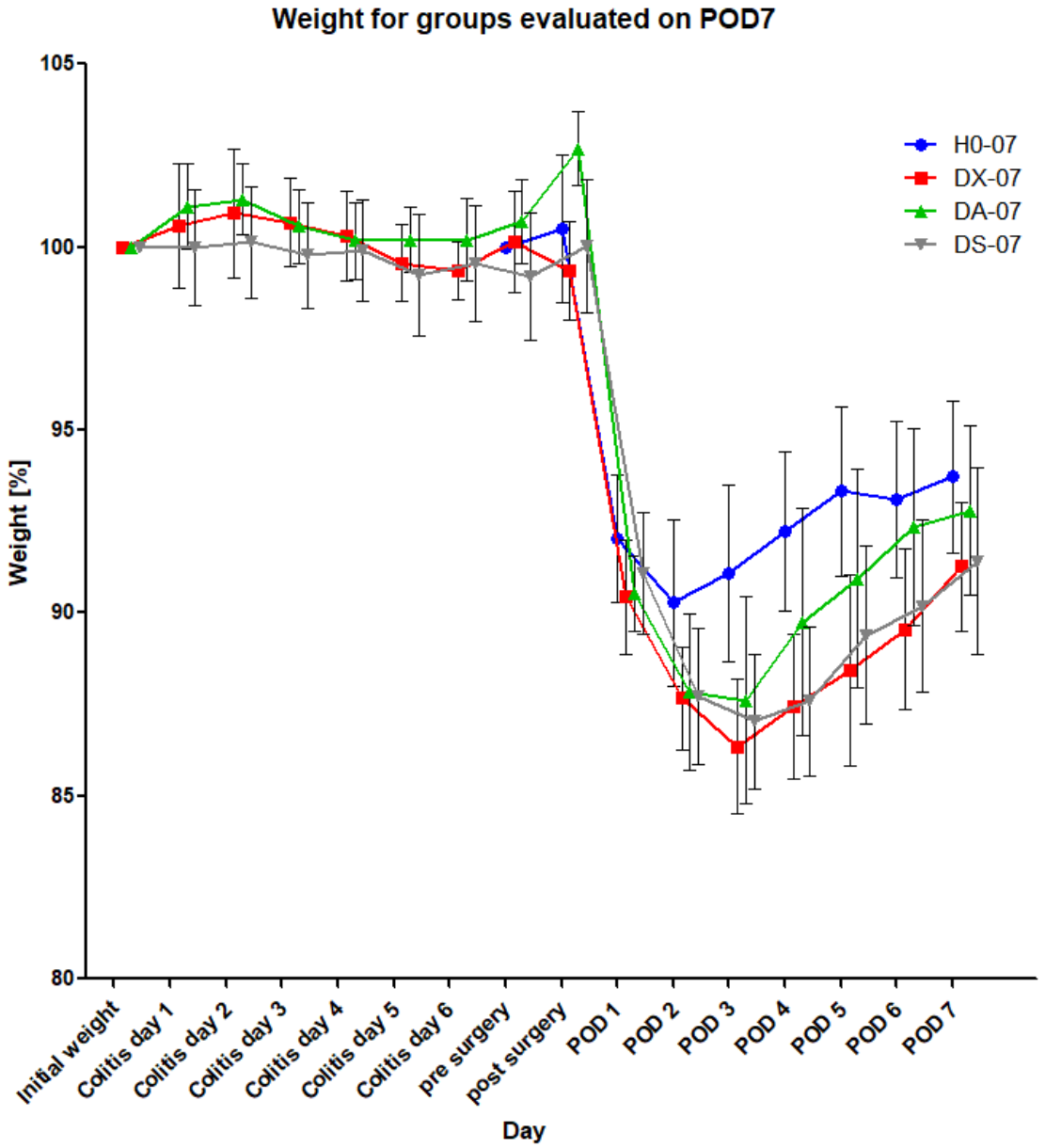

Figure 21: Mean weight curves for H0, DX, DA and DS groups evaluated on POD7.

Group designations: H0: water control group; surgery without DSS-colitis or treatment. DX: DSS-control group; DSS-colitis with 2%, surgery, no treatment. DS: scramble-control group; DSS-colitis with 2%, surgery, sham treatment with Scrm-NPs. DA: experiment group; DSS-colitis with 2%, surgery, treatment with Ac2-26 NPs.

The bars signify the 95% confidence interval. Note that no weight measurements have been taken for the H0 group until the preoperative measurement, since there is no colitis induction phase. The weight of the animals in the colitis groups is distributed around 100% of the initial weight during induction of DSS colitis, followed by a distinct drop of 10-15% after surgery. Weight curves reach a nadir on POD2 to POD3 followed by partial recovery.
Own figure based on experimental data.

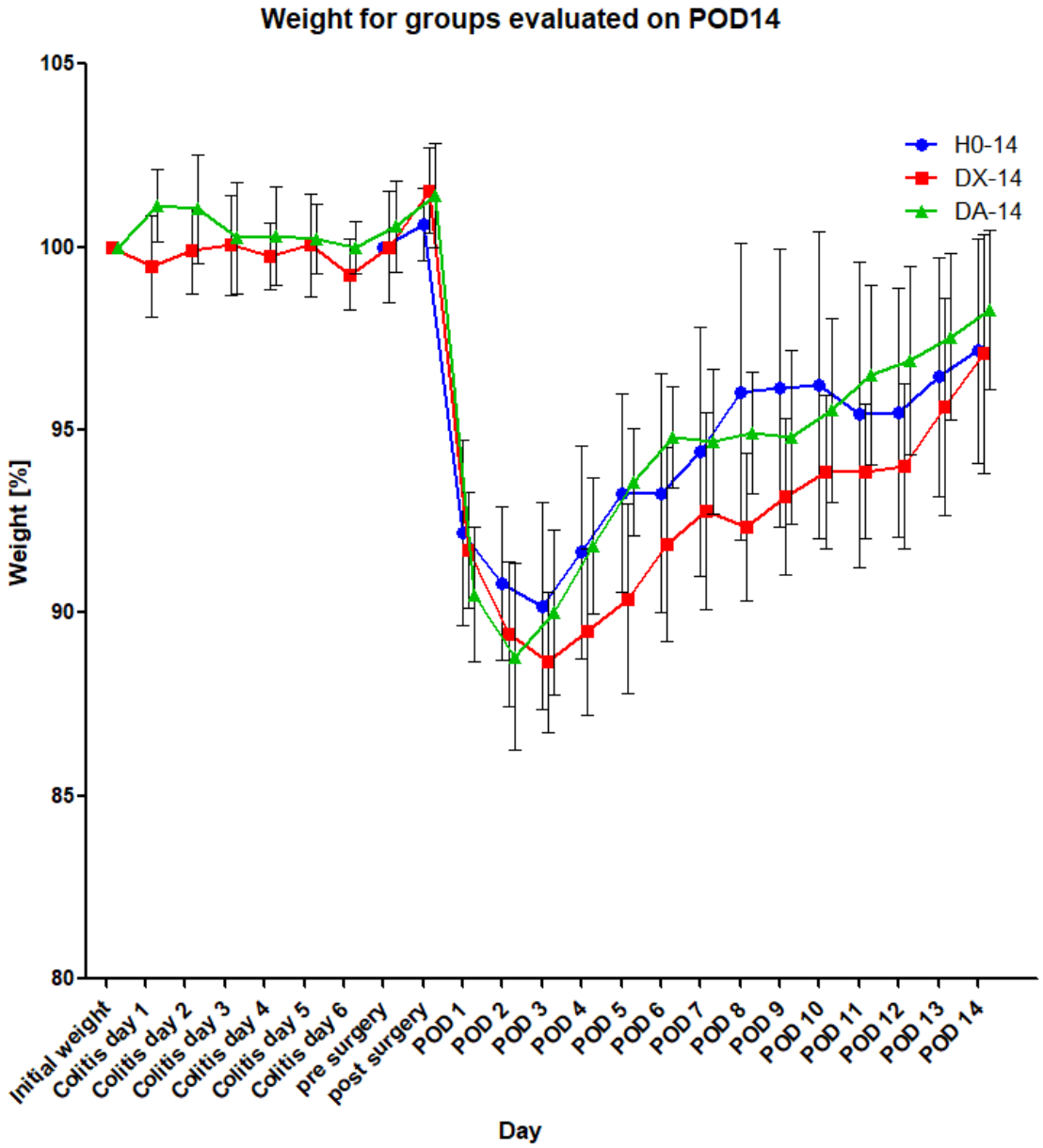

Figure 22: Mean weight curves for H0, DX, DA groups evaluated on POD14.

Group designations: H0: water control group; surgery without DSS-colitis or treatment. DX: DSS-control group; DSS-colitis with 2%, surgery, no treatment. DA: experiment group; DSS-colitis with 2%, surgery, treatment with Ac2-26 NPs.

The bars signify the 95% confidence interval. Note that no weight measurements have been taken for the H0 group until the pre-operative measurement, since there is no colitis induction phase. The weight of the animals in the colitis groups is distributed around 100% of the initial weight during induction of DSS colitis, followed by a distinct drop of 10-15% after surgery.
Own figure based on experimental data.

For the DSS colitis groups, the weight is distributed around 100% of the baseline during induction of colitis. This is followed by a sharp drop of about 10-15% after surgery. It is noteworthy that this decrease in weight cannot be attributed to perioperative loss of fluid, since the average immediate postoperative weight measurements tend to be within -1% to +2% of preoperative weight.

Group	Mean pre-operative weight	Mean post-operative weight	Balance		Significance level	p
H0-03	100.00%	99.11%	-	0.89%	ns	*0.0933*
H0-07	100.00%	100.49%	+	0.49%	ns	*0.5974*
H0-14	100.00%	100.62%	+	0.62%	ns	*0.1992*
DX-03	99.84%	99.61%	-	0.23%	ns	*0.7794*
DX-07	100.14%	99.35%	-	0.79%	ns	*0.3469*
DX-14	99.98%	101.54%	+	1.57%	*	***0.0156***
DA-03	100.96%	102.16%	+	1.19%	*	***0.0181***
DA-07	100.69%	102.70%	+	2.00%	**	***0.0013***
DA-14	100.58%	101.40%	+	0.82%	ns	*0.1349*
DS-03	99.05%	99.06%	+	0.01%	ns	*0.9600*
DS-07	99.16%	100.04%	+	0.88%	ns	*0.2802*

Table 7: Analysis of average pre- and postoperative weight in percent of the baseline weight.

Group designations: H0: water control group; surgery without DSS-colitis or treatment. DX: DSS-control group; DSS-colitis with 2%, surgery, no treatment. DA: experiment group; DSS-colitis with 2%, surgery, treatment with Ac2-26 NPs. Significance has been determined by paired t-tests between groups. ns=non-significant, *=significant on a 95% level, **=significant on a 99% level, ***=significant on a 99.9% level.
Own table based on experimental data.

The only significant differences occur in groups DX-14, DA-03 and DA-07. In all these groups, the balance is slightly positive. This is an indicator that the perioperative irrigation strategy (see 2.2.6) compensated intraoperative loss of fluid in most cases and over-compensated it in some.

The weight curves reach a nadir around POD3, followed by recovery. Unpaired t-tests have been calculated between groups on every POD. To avoid overloading the figures with information, the results of significance analysis have been collected in Table 8.

Groups		p for POD													
		1	2	3	4	5	6	7	8	9	10	11	12	13	14
H0-03	DX-03	ns	ns	ns											
H0-03	DA-03	*	ns	ns											
H0-03	DS-03	ns	*	ns											
DX-03	DA-03	*	ns	ns											
DX-03	DS-03	*	*	ns											
DA-03	DS-03	ns	ns	ns											
H0-07	DX-07	ns	*	**	**	**	*	ns							
H0-07	DA-07	ns	ns	ns	ns	ns	ns	ns							
H0-07	DS-07	ns	ns	**	**	*	ns	ns							
DX-07	DA-07	ns	ns	ns	ns	ns	ns	ns							
DX-07	DS-07	ns	ns	ns	ns	ns	ns	ns							
DA-07	DS-07	ns	ns	ns	ns	ns	ns	ns							
H0-14	DX-14	ns	ns	ns	ns	ns	ns	ns	ns	ns	ns	ns	ns	ns	ns
H0-14	DA-14	ns	ns	ns	ns	ns	ns	ns	ns	ns	ns	ns	ns	ns	ns
DX-14	DA-14	ns	ns	ns	ns	*	*	ns	*	ns	ns	ns	ns	ns	ns

Table 8: Statistical analysis of the differences in weight between the groups.

Group designations: H0: water control group; surgery without DSS-colitis or treatment. DX: DSS-control group; DSS-colitis with 2%, surgery, no treatment. DA: experiment group; DSS-colitis with 2%, surgery, treatment with Ac2-26 NPs. Significance has been determined by unpaired t-tests between groups on the PODs indicated. ns=non-significant, *=significant on a 95% level, **=significant on a 99% level, ***=significant on a 99.9% level.
Own table based on experimental data.

There are significant differences mainly between the groups H0-07 and DX-07 resp. DS-07 in the first 7 postoperative days. H0 groups evaluated on POD7 and 14 recover weight faster than the DX and DS groups. The DA groups lies in between these extremes; however, the differences are not significant, except for the DA-14 and DX-14 groups on POD5, 6 and 8.

3.3.2. Adhesion formation

Histograms of adhesion scores are shown in Figure 23 for the H0- (surgery, no colitis, no treatment), DX- (DSS colitis, surgery, no treatment), DS- (DSS colitis, surgery, sham

treatment with i.p. injections of Scrm-NP) and DA-group (DSS colitis, surgery, treatment by i.p. injections of Ac2-26-NP) on POD3, 7 and 14. Like most scores, the adhesion score is ordinal scaled. Therefore, the median should be the preferred averaging method.

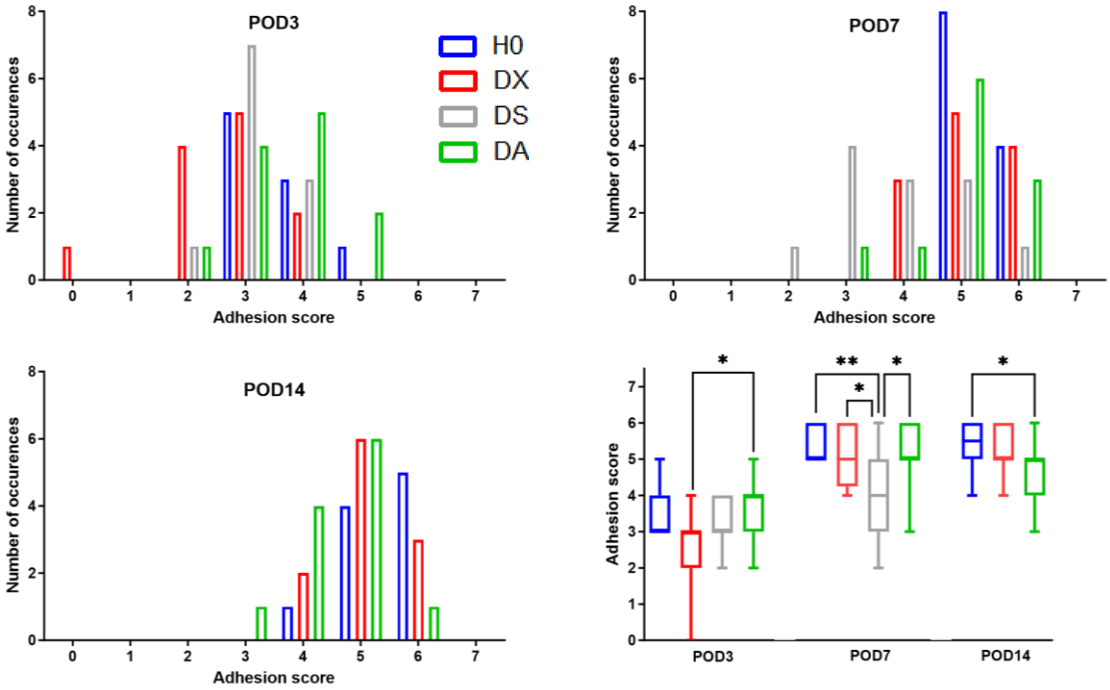

Figure 23: Histograms and medians of adhesion scores.

Group designations: H0: water control group; surgery without DSS-colitis or treatment. DX: DSS-control group; DSS-colitis with 2%, surgery, no treatment. DS: scramble-control group; DSS-colitis with 2%, surgery, sham treatment with Scrm-NPs. DA: experiment group; DSS-colitis with 2%, surgery, treatment with Ac2-26 NPs. Histograms of adhesion scores on the top and bottom left for POD3, 7 and 14. Boxplots for each group on the different days on the bottom right. Significance bars for comparison between groups on each day: *=significant on a 95% level, **=significant on a 99% level, ***=significant on a 99.9% level.
Own figure based on experimental data.

Not all distributions approximate a gaussian curve, so the Mann-Whitney-U-test is more suitable than a t-test. The results are shown in Table 9. The medians on POD3 lie at 3 for H0, DX and DS group, whereas the DA group has a median of 4. The difference in median between DX and DA group is significant on a 95% confidence level, the differences between the other groups are not significant.

On POD7, the medians are higher: a score of 5 for H0, DX and DA group, 4 for DS group. The differences between H0 and DS group are significant on a 99% confidence level, the differences between DX and DS group as well as between DA and DS group are significant on a 95% level.

On POD14, the H0 group has a median score of 5.5, DX and DA groups of 5. Only the difference between the H0 and DA group is significant on a 95% level.

There are also the differences in one group between the medians on the different PODs to consider: Within the H0 and DX groups, the differences between POD3 and 7 as well

as the differences between POD3 and 14 are significant on a 99.9% confidence level, the differences between POD7 and 14 are not significant.

Within the DS groups, the differences between POD3 and 7 are not significant. Within the DA groups, the difference between POD3 and 7 is significant on a 99% level, the difference between POD3 and 14 on a 95% level.

Group	H0-03	H0-07	H0-14	DX-03	DX-07	DX-14	DA-03	DA-07	DA-14	DS-03	DS-07
H0-03		***	***	*			ns			ns	
H0-07	***		ns		ns			ns			**
H0-14	***	ns				ns			*		
DX-03	*				***	***	*			ns	
DX-07		ns		***		ns		ns			*
DX-14			ns	***	ns				ns		
DA-03	ns			*				**	*	ns	
DA-07		ns			ns		**		ns		*
DA-14			*			ns	*	ns			
DS-03	ns			ns			ns				ns
DS-07		**			*			*		ns	

Table 9: Significance levels between the adhesion scores of groups computed using Mann-Whitney-U.

Group designations: H0: water control group; surgery without DSS-colitis or treatment. DX: DSS-control group; DSS-colitis with 2%, surgery, no treatment. DA: experiment group; DSS-colitis with 2%, surgery, treatment with Ac2-26 NPs. Non-plausible comparisons (group with itself, different groups for different days) have been greyed out. ns=non-significant, *=significant on a 95% level, **=significant on a 99% level, ***=significant on a 99.9% level.
Own table based on experimental data.

3.3.3. Endoscopic healing

Endoscopic healing score distributions for the H0- (surgery, no colitis, no treatment), DX- (DSS colitis, surgery, no treatment) and DA-groups (DSS colitis, surgery, treatment by i.p. injections of Ac2-26-NP) are shown as histograms for POD3, 7 and 14 in Figure 24. These distributions deviate further from a gaussian distribution than those of the adhesion scores. The endoscopic healing score is ordinal scaled. Therefore, the median should be the preferred averaging method. Significance was calculated using Mann-Whitney-U test.

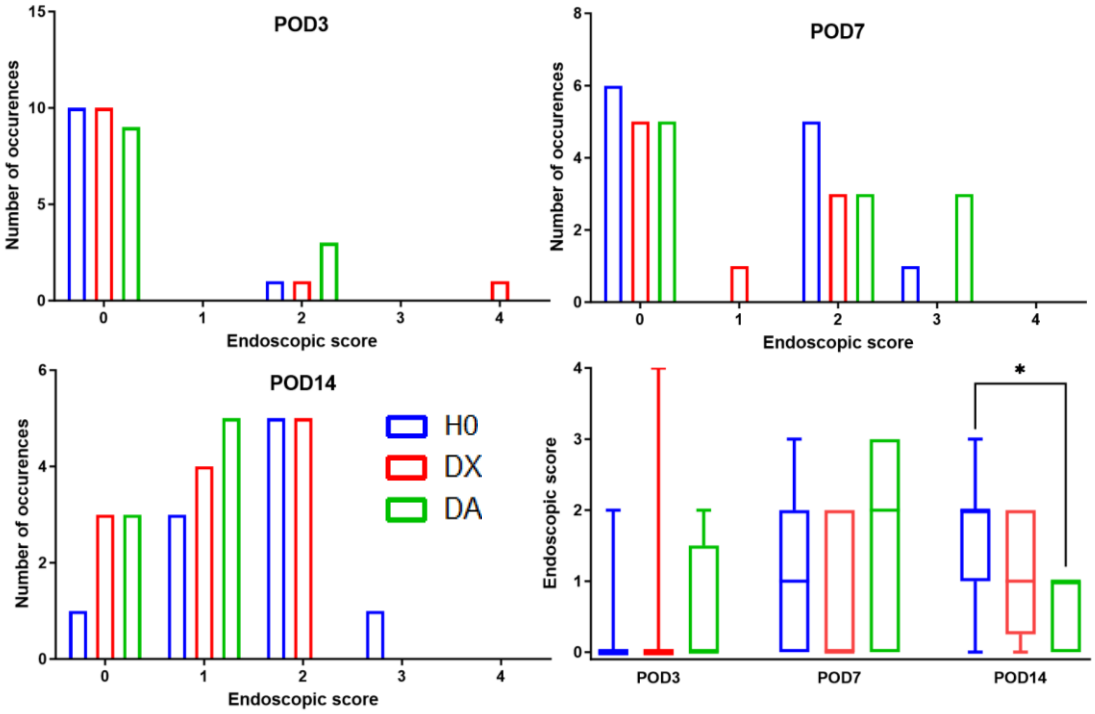

Figure 24: Histograms and medians of endoscopic healing scores.

Group designations: H0: water control group; surgery without DSS-colitis or treatment. DX: DSS-control group; DSS-colitis with 2%, surgery, no treatment. DA: experiment group; DSS-colitis with 2%, surgery, treatment with Ac2-26 NPs. Histograms of endoscopic scores on POD3, 7 and 14 on the top and bottom left. Boxplots for each group on POD3, 7 and 14 on the bottom right. Significance bars for comparison between groups on each day: *=significant on a 95% level, **=significant on a 99% level, ***=significant on a 99.9% level.
Own figure based on experimental data.

The medians for POD3 lie at 0 for all groups with no significant difference between groups. On POD7, the median for H0 group is 1, whereas the median score for group DX is 0 and 2 for DA group. These differences are not significant, however. The median endoscopic healing scores for the H0 group is 2 on POD14, for DX and DA group it is 1. The difference in scores between H0 and DA is significant on a 95% level.

Within the groups, the difference between POD3 and 7 is significant on a 95% level for H0 group. The differences between POD3 and 14 are significant on a 99.9% level for group H0 and on a 95% level for group DX. The other differences are not significant.

Group	H0-03	H0-07	H0-14	DX-03	DX-07	DX-14	DA-03	DA-07	DA-14
H0-03		*	***	ns			ns		
H0-07	*		ns		ns			ns	
H0-14	***	ns				ns			*
DX-03	ns				ns	*	ns		
DX-07		ns		ns		ns		ns	
DX-14			ns	*	ns				ns
DA-03	ns			ns				ns	ns
DA-07		ns			ns		ns		ns
DA-14			*			ns	ns	ns	

Table 10: Significance levels between the endoscopic healing scores of groups computed using Mann-Whitney-U.

Group designations: H0: water control group; surgery without DSS-colitis or treatment. DX: DSS-control group; DSS-colitis with 2%, surgery, no treatment. DA: experiment group; DSS-colitis with 2%, surgery, treatment with Ac2-26 NPs. Non-plausible comparisons have been greyed out. ns=non-significant, *=significant on a 95% level, **=significant on a 99% level, ***=significant on a 99.9% level.
Own table based on experimental data.

3.3.4. Histopathological healing score

The results of histopathological scoring (see 2.2.8.5) of the H0- (surgery, no colitis, no treatment), DX- (DSS colitis, surgery, no treatment) and DA-group (DSS colitis, surgery, treatment by i.p. injections of Ac2-26-NP) on POD3, 7 and 14 is shown in Figure 25.

The asymmetric distribution of box and whisker bounds is an indicator for non-gaussian distribution of values. As most scores, the histopathological score is ordinal scaled. Therefore, the median should be the preferred averaging method. Significance was calculated using Mann-Whitney-U test.

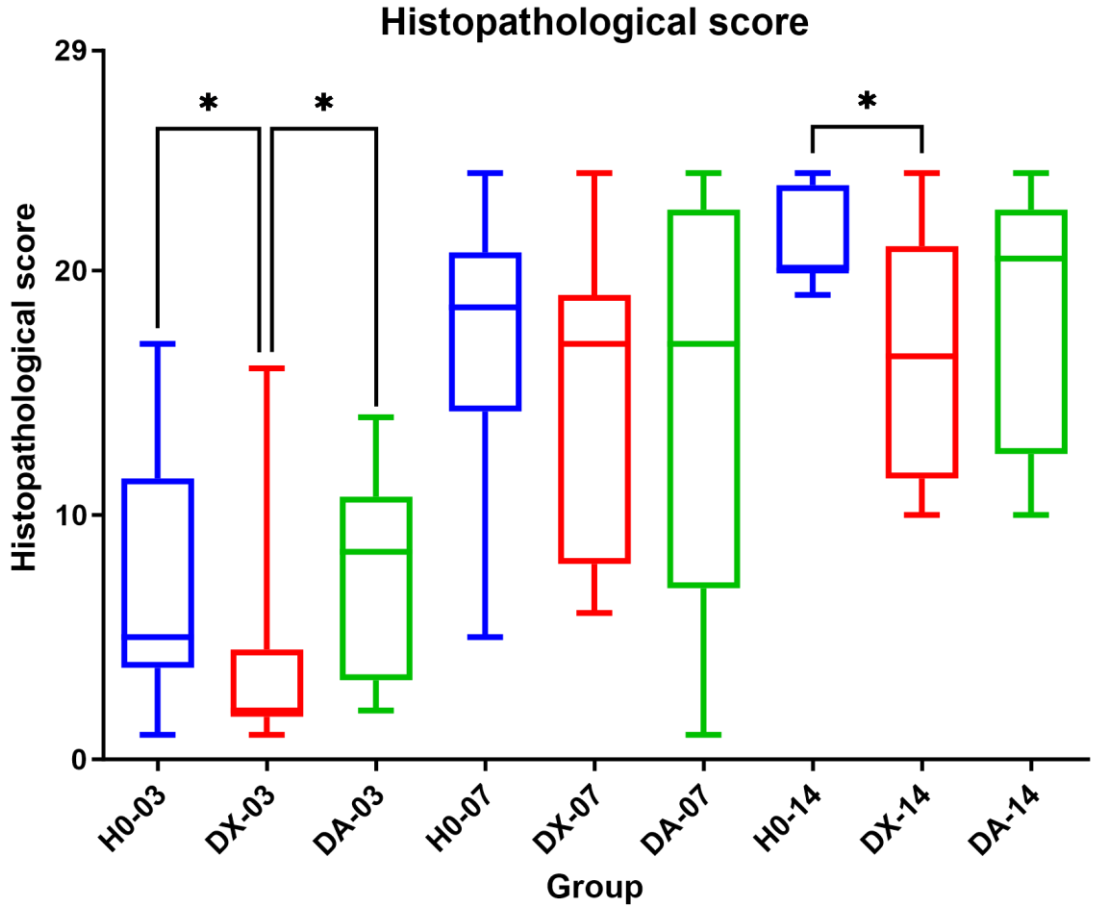

Figure 25: Boxplots of histopathological scores of different groups on POD3, 7 and 14.

Group designations: H0: water control group; surgery without DSS-colitis or treatment. DX: DSS-control group; DSS-colitis with 2%, surgery, no treatment. DA: experiment group; DSS-colitis with 2%, surgery, treatment with Ac2-26 NPs. The upper and lower bounds of boxes signify first and third quartile, the line within the box is the median. The whiskers signify the 95% confidence interval. To avoid overloading the figure with information, the significance indicators between subgroups of the same experiment group with evaluation on different PODs (i.e., H0-03 vs H0-07) have been left out.
Own figure based on experimental data.

On POD3, the median of the H0 group lies at 5 score points, that of the DX group at 2 and of DA at 8.5. The differences between the H0 and the DX group as well as between DX and DA group are significant on a 95% level, but the difference between H0 and DA is not.

On POD7, the medians of the groups are: H0: 18.5; DX: 17; DA: 17 score points. There are no significant differences.

The median of H0 group on POD14 is 20. DX has a median score of 16.5 whereas the median score of the DA group is 20.5. The difference between H0 and DX is significant on a 95% level, whereas the differences between DX and DA or between H0 and DA are not.

Group	H0-03	H0-07	H0-14	DX-03	DX-07	DX-14	DA-03	DA-07	DA-14
H0-03		**	***	*			ns		
H0-07	**		*		ns			ns	
H0-14	***	*				ns			ns
DX-03	*				***	***	*		
DX-07		ns		***		ns		ns	
DX-14			ns	***	ns				ns
DA-03	ns			*				*	**
DA-07		ns			ns		*		ns
DA-14			ns			ns	**	ns	

Table 11: Significance levels of the differences between the histopathological scores of groups computed using Mann-Whitney-U.

Group designations: H0: water control group; surgery without DSS-colitis or treatment. DX: DSS-control group; DSS-colitis with 2%, surgery, no treatment. DA: experiment group; DSS-colitis with 2%, surgery, treatment with Ac2-26 NPs. Non-plausible comparisons have been greyed out. ns=non-significant, *=significant on a 95% level, **=significant on a 99% level, ***=significant on a 99.9% level.
Own table based on experimental data.

3.3.5. Bursting pressures

When comparing bursting pressures, it must first be considered where the bursting occurs. Figure 26 shows relative frequency of bursting locations for H0- (surgery, no colitis, no treatment), DX- (DSS colitis, surgery, no treatment) and DA-group (DSS colitis, surgery, treatment by i.p. injections of Ac2-26-NP) on POD3, 7 and 14. Whereas on POD3 bursts frequently happen at the site of anastomosis as well as remote from it, from POD7 on most bursts happen remote from it. This trend continues up to POD14 where only one anastomosis in the DA group actually burst at the site of anastomosis.

Figure 27 shows boxplots of bursting pressures in mmHg for the four experiment groups on POD3 (top), POD7 (middle) and POD14 (bottom). The graphs on the left show the total distribution of bursting pressures without any differentiation as to bursting location, whereas in the graphs on the right-hand side the results have been divided in values measured with bursts at the site of the anastomosis and ones in which the burst has occurred remote from it. In case of only one single measurement (H0-07, DX-07 and DA-14), no box plot could reasonably be compiled. In these instances, the single value is given instead.

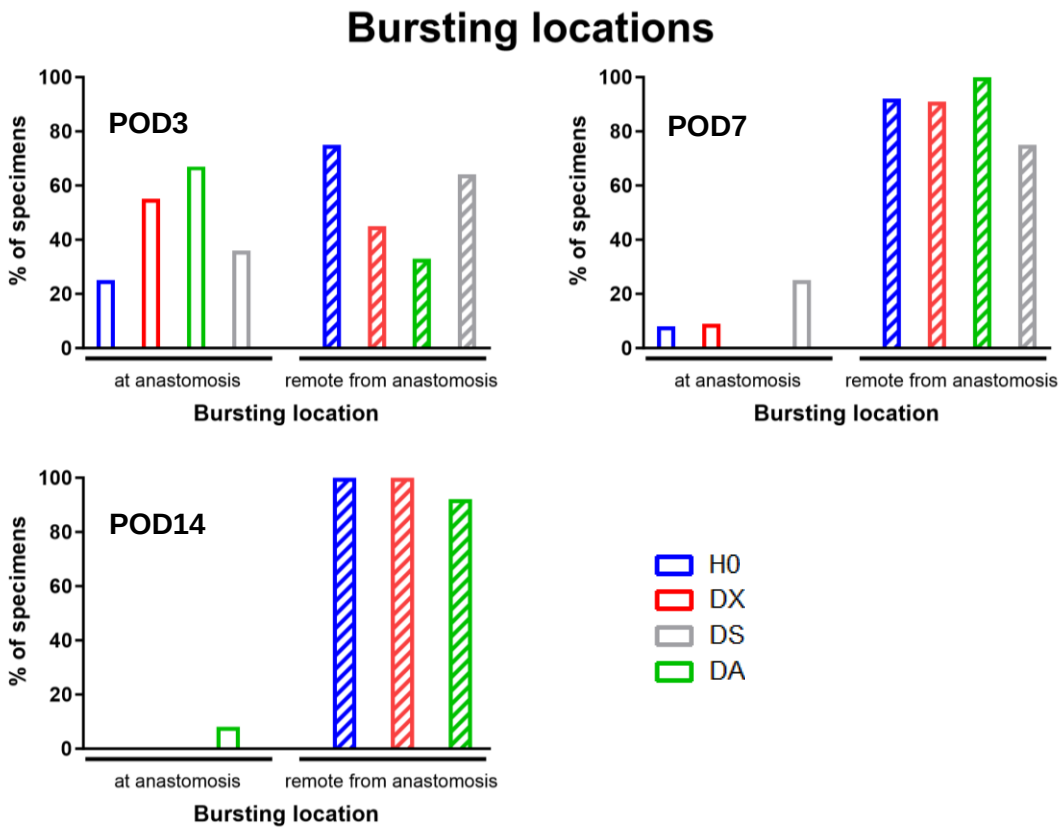

Figure 26: Bar graphs of relative frequency of bursting at the site of anastomosis or remote from it in the groups H0, DX, DS and DA on POD3, 7 and 14.

Group designations: H0: water control group; surgery without DSS-colitis or treatment. DX: DSS-control group; DSS-colitis with 2%, surgery, no treatment. DS: scramble-control group; DSS-colitis with 2%, surgery, sham treatment with Scrm-NPs. DA: experiment group; DSS-colitis with 2%, surgery, treatment with Ac2-26 NPs.
Own figure based on experimental data.

Whereas on POD3 the average bursting pressures for all group lie below 100 mmHg, on POD7 and POD14 the values are distributed around 150 mmHg. The only significant difference exists between H0 and DS on POD3 (99% significance level) if the groups are compared without regard for the site of bursting. The significance vanishes when the subgroups with bursting location at or remote from the anastomosis are compared. On POD3, the differences between the measurements within the same group are not significantly different comparing bursting at and remote from the site of anastomosis. Due to the low number of bursts at the actual site of anastomosis on POD7 and POD14, a statistical analysis here is not very reasonable.

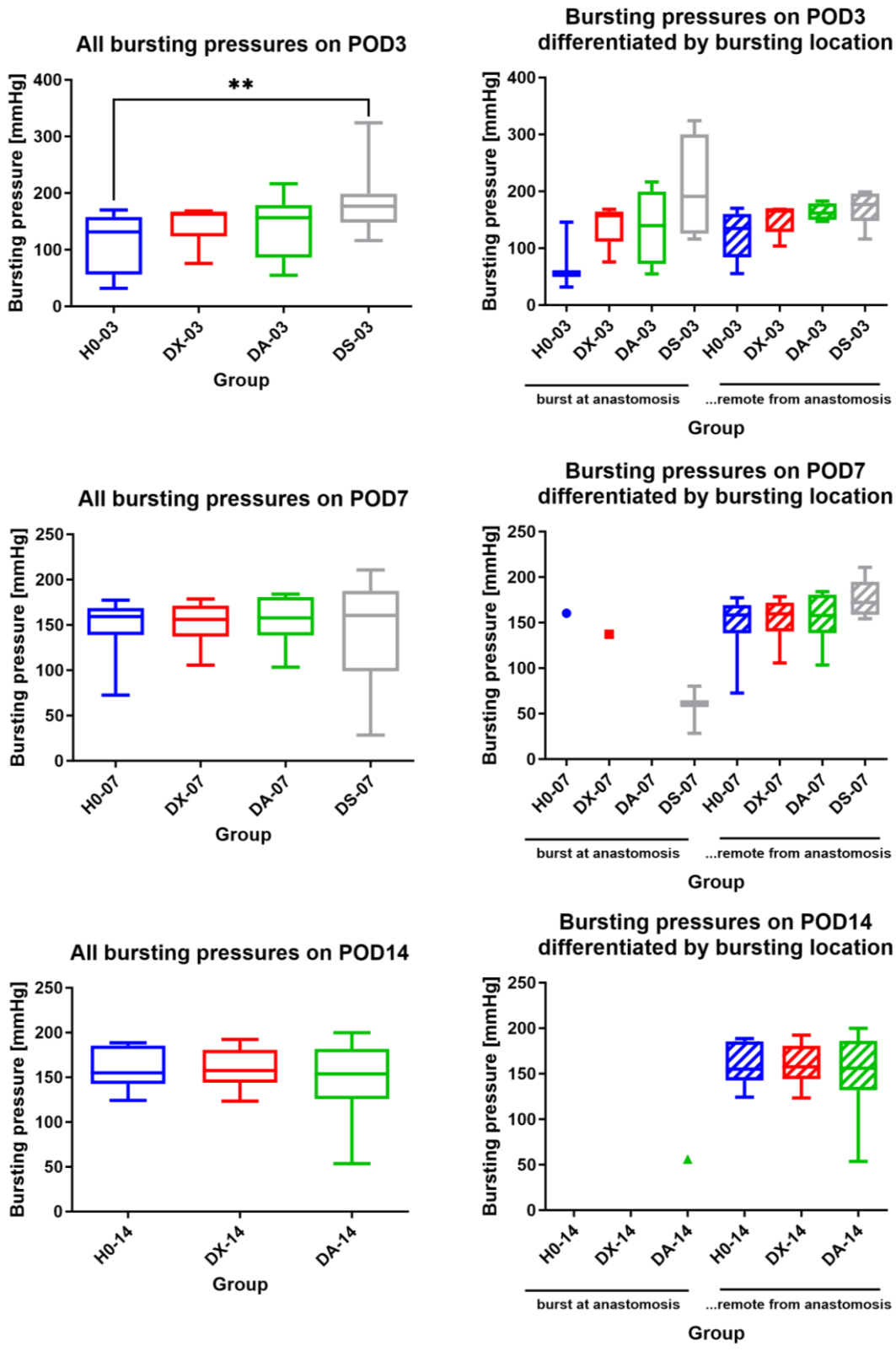

Figure 27: Boxplots of bursting pressures for H0, DX, DS and DA group.

Group designations: H0: water control group; surgery without DSS-colitis or treatment. DX: DSS-control group; DSS-colitis with 2%, surgery, no treatment. DS: scramble-control group; DSS-colitis with 2%, surgery, sham treatment with Scrm-NPs. DA: experiment group; DSS-colitis with 2%, surgery, treatment with Ac2-26 NPs. Evaluation on POD3 (top), POD7 (middle) and for H0, DX and DA on POD14 (bottom). Total distribution of bursting pressures on the left. Results divided in values measured with bursts at the site of the anastomosis and remote from it on the right. Upper and lower bound of boxes signify 1. and 3. quartile, the line in the box is the arithmetic mean. Whiskers signify 95% confidence interval. In case of only one single measurement, no box plot could reasonably be compiled. In these instances, the single value is given instead.
Own figure based on experimental data.

4. Discussion

4.1. Goals achieved

4.1.1. DSS Dose-finding and D0 group

In the experiments conducted to best adapt the induction dose of DSS to the conditions such as mouse strain, microbiome in our lab etc., we could not find a correlation between the DAI and the histological colitis score. Relying on loss of weight after 7 days of exposure to DSS as a simpler, clinical parameter, we derived the (in retrospect, incorrect) conclusion, that in our laboratory setting, we needed as high a concentration of 5% of DSS to yield sufficient inflammation. We started the D0 group on an induction with 5% of DSS in drinking water for 7 days, followed by surgery.

However, this D0 group proved insupportable. Minor complications during surgery could not explain the alarming abort rates since they were both equally present in the successful and unsuccessful animals. This caused us to consider excessive DSS colitis as the cause of the bad clinical state of the mice and to re-evaluate the induction process. We found that very likely the D2 to D5 groups were evaluated too early and that in the D0 group the full amount of colitis only started to cause clinical symptoms after switching to normal water. This effect had caused us to underestimate the severity of colitis in our D0 group. In the subsequent DX group, we tried 2% of DSS for induction as recommended (Wirtz, Neufert et al. 2007). This yielded a sufficient DSS colitis as we ascertained through preoperative endoscopies. We continued with 2% of DSS in the DA and DS groups.

4.1.2. Interpretation of results with Ac2-26-loaded nanoparticles

The weight measurements presented in 3.3.1 show stable weight curves during induction of colitis, stable perioperative weight with a slight over-compensation of perioperative loss of fluid in some cases. This is followed by a marked weight loss with a nadir around POD3 with gradual, partial recovery which is still in process on POD14. Mice without colitis (H0 group) make a rather swift recovery compared to groups affected with colitis and receiving no or only sham treatment (DX and DS group). The difference is significant in the groups with evaluation on POD7 for POD3 to 5. The treatment group (DA) which had received i.p. injections of Ac2-26-NP lies in between and recovers better than the DX and DS groups – although this effect could only be shown to be significant at several isolated PODs with the group size of 12 animals considered here.

The H0 and DX groups show a steady, significant rise in adhesions from endpoint on POD3 to POD14. The DS group has significantly less adhesions on POD7. Interestingly, the DA group shows significantly increased adhesion formation on POD3, 7 and 14 compared to the untreated groups with a significant increase of adhesion formation within the DA group from POD3 to 14. These findings are yet unexplained since adhesions are usually not regarded as beneficial to successful healing and the group which is expected to heal best in this experiment showed the most adhesions. One possible key to clearing this open question might be the addition of a classification of abscess formation as proposed in (Miltschitzky, Clees et al. 2021) in order to be able to correlate findings on septic complications as abscess formation or peritonitis with adhesion formation to determine if adhesions formed in the course of defense against infection or for some other reason.

There are no great inter-group differences in endoscopic healing on any given POD apart from a significant difference between the untreated, H0 group and the treatment group DA. However, the scores are rising significantly within the groups towards POD14 – and higher scores mean more dehiscence. This is an unexpected result, since based on published literature on the subject, anastomotic dehiscence would rather be expected in the earlier healing phases (Thornton and Barbul 1997). The finding cannot be explained as a late effect of earlier disruption of the healing process by perpetuated inflammation with an insufficient proliferative phase, since the effect is strongest in the H0 group in which there was no colitis present. One possible cause might be too tight sutures which restrict blood flow direly needed for successful healing. This effect would be seen strongly during the proliferative phase, in which nutrients and cells need to be transported into the healing tissue in large quantities. This hypothesis could be tackled in another experiment, which assays the perfusion through contrast enhanced *in vivo* imaging. The findings of higher-than-physiological pressure tolerance of the anastomoses from bursting pressure measurements (see 4.1.3) suggest that the mechanical strength of the anastomosis can be reduced without leading to native insufficiency.

The results from the evaluation of histopathological healing as presented in 3.3.4, however, show a different development. As expected, there is a significant progress of wound healing within the first 7 postoperative days in all groups. However, the DA group already shows significantly better healing on POD3 compared to the DX group. The difference between these groups is not significant at POD14 anymore, however, the difference between the DX and H0 group is significant at POD3 and 14. This means that the DX group does not quite catch up after initially delayed healing, whereas the DA group is off to a better start on a molecular level. These findings are congruent with studies presented in

1.1.2 and 1.2.2 which demonstrate the importance of timely resolution of inflammation in the early phases of anastomotic healing and the strong, beneficial effect Ac2-26 can exert there.

4.1.3. Critical review of bursting pressure measurement

Some publications interpret the definition of successful anastomotic healing by mechanical cohesion (see 1.1.2) in such a way that they rely heavily on measuring the anastomotic strength indicated by the bursting pressure (Fukuchi, Seeburger et al. 1999, Migaly, Lieberman et al. 2004). While this approach provides an easily obtainable determinant and reflects that mechanical interruption of tissue continuity at the site of anastomosis invariably causes acute AL, it does not consider the necessity for microscopic changes like re-epithelialization for full restitution of a functional intestine that can be observed by pathological examination of the tissue surrounding the anastomosis only. Also, pressure in the fluid-filled intestine will most likely cause the intestine to burst in the place of least mechanical stability. If this is the site anastomosis, bursting can be expected there. If, however, the anastomosis equals or exceeds the stability of the intestine around it, the burst happens at some other place. In this case, the mechanical stability of the anastomosis does not equal the bursting pressure measured – this is merely the lower limit.

In the experiments presented here, bursting pressure measurement were truly valid only on POD3, since at later endpoints almost all bursts occurred at a remote part of the intestine instead of at the site of anastomosis. Moreover, the bursting pressures of 100 mmHg and above are in a non-physiological pressure range for the intestine. This also raises the question if the bursting pressure measurement actually measures a physiologically vital parameter – an anastomosis which bursts at e.g., 50 mmHg would be in the bottom 25% of the values observed on POD3. Yet under physiological conditions the intestine might never be exposed to so much stress and the anastomosis might be perfectly stable *in vivo*. Therefore, a measure of caution should be applied when considering results obtained by measuring bursting pressure only.

4.2. Further research opportunities

In addition to the results discussed here, several promising avenues of research can be pursued starting from the project presented in this thesis:

4.2.1. Automatized colitis scoring

Since the histological colitis scoring process takes a lot of man-hours by personnel with pathological training, automatization of this task promises immense benefits to colitis-related research. Rather surprisingly given the high relevance of DSS colitis in recent research, we were only able to find one publication about such an effort which has been made to date. This project used an object-oriented program with fixed rules for image analysis and scoring (Kozlowski, Jeet et al. 2013). However, it is often hard for pathologists to point out what makes the difference between healthy and injured mucosa in their scoring – the trained eye can just see the difference. Therefore, we devised a project to train a neuronal network to score Swiss rolls on a large number of pre-scored slides instead of creating a fixed framework of rules to develop a fast, well-trained expert system which can score Swiss rolls consistently and thus to automatize a time-consuming chore of research into IBD.

We have been able to acquire the startup company scalable minds GmbH (https://scalableminds.com/) as a partner for this project. They have profound experience in AI-related research and its application in science and had already demonstrated the project's feasibility. Lacking sufficient funding, we could not pursue the project further yet.

4.2.2. Adapting the setup to different models of colitis and different modes of application

To differentiate between the effects perpetuated inflammation of any kind exerts on anastomotic healing from DSS-colitis-specific inhibition of healing processes, it is necessary to add control groups with different methods of inducing colitis. Indeed, the next experiment setup by R. L. Walter and V. Vieregge after the completion DS group also included groups with TNBS instead of DSS colitis.

A very important step on the road to an eventual translation into clinical use of nanoparticles delivering Ac2-26 or similar mediators might depend on researching alternative ways of delivering the drug into the target tissue. Since this tissue is accessible from the lumen of the intestine, oral application might help limiting the systemic effect and increase the local concentration. The experiments presented here could be performed in an adapted fashion, using an additional layer of pectin coating on the nanoparticles to protect them from gastric passage and release them in the large intestine by bacterial digestion of the pectin coat. Another possible strategy might be to coat suture material with Ac2-26 nanoparticles to facilitate their local release at the site of anastomotic healing.

5. Conclusion

Septic complications, such as anastomotic leakage, represent major surgical complications in surgery for inflammatory bowel disease. The problem is decades old, but there still are profound gaps in our knowledge of the processes involved. Especially the complex processes involved in anastomotic healing during inflammatory conditions are only incompletely understood.

SPMs are potent anti-inflammatory and pro-resolution mediators, inviting the scientist and clinician alike to further explore their potential. Even though doctors influence SPM- and Annexin dependent pathways in patients with natural salicylates since millennia, since the late 19th century with aspirin and since the 1940's through corticosteroids, the full extent of the relevant downstream mediators is yet elusive and provides ample opportunity for further research.

Of course, the effect of mediators on specific cell populations can be researched in cell cultures, but it is not possible to simulate the entire intestine *ex vivo*. This means that animal experiments will remain the backbone of this research for the near future.

The experimental setup developed in the course of this thesis is a standardized, reproducible mouse model combining preoperative colitis and colorectal surgery. It allows monitoring of anastomotic healing during inflammatory conditions through functional outcomes, clinical scores, endoscopy and histopathological examination as well as molecular analysis of tissues (e.g., Western Blot, RNA analysis). It offers the potential for improved reporting of findings and allows testing various mediators for post-operative healing. While refining and reducing animal experiments, this platform is planned to enable scientists to achieve the direly needed breakthroughs in colorectal surgery – a goal which it has already served to some extent: In the experiments published in (Reischl, Lee et al. 2021), the potency of targeted Ac2-26 nanoparticles to significantly improve anastomotic healing under adverse, inflammatory conditions could be shown. Subsequent molecular analysis of the samples generated led to the new insights into the downstream processes which can nudge the tissue to successful healing.

Appendix

Table of Figures and Tables

References

1. Peeters, K.C., et al., *Risk factors for anastomotic failure after total mesorectal excision of rectal cancer.* Br J Surg, 2005. **92**(2): p. 211-6.
2. Thompson, S.K., E.Y. Chang, and B.A. Jobe, *Clinical review: Healing in gastrointestinal anastomoses, part I.* Microsurgery, 2006. **26**(3): p. 131-6.
3. Krarup, P.M., et al., *Anastomotic leak increases distant recurrence and long-term mortality after curative resection for colonic cancer: a nationwide cohort study.* Ann Surg, 2014. **259**(5): p. 930-8.
4. Gessler, B., O. Eriksson, and E. Angenete, *Diagnosis, treatment, and consequences of anastomotic leakage in colorectal surgery.* Int J Colorectal Dis, 2017. **32**(4): p. 549-556.
5. Law, W.L., et al., *Anastomotic leakage is associated with poor long-term outcome in patients after curative colorectal resection for malignancy.* J Gastrointest Surg, 2007. **11**(1): p. 8-15.
6. Choi, H.K., W.L. Law, and J.W. Ho, *Leakage after resection and intraperitoneal anastomosis for colorectal malignancy: analysis of risk factors.* Dis Colon Rectum, 2006. **49**(11): p. 1719-25.
7. Khan, A.A., et al., *The management and outcome of anastomotic leaks in colorectal surgery.* Colorectal Dis, 2008. **10**(6): p. 587-92.
8. Paun, B.C., et al., *Postoperative complications following surgery for rectal cancer.* Ann Surg, 2010. **251**(5): p. 807-18.
9. Smith, J.A., et al., *Evidence of the effect of 'specialization' on the management, surgical outcome and survival from colorectal cancer in Wessex.* Br J Surg, 2003. **90**(5): p. 583-92.
10. Matthiessen, P., et al., *Defunctioning stoma reduces symptomatic anastomotic leakage after low anterior resection of the rectum for cancer: a randomized multicenter trial.* Ann Surg, 2007. **246**(2): p. 207-14.
11. Krarup, P.M., et al., *A nationwide study on anastomotic leakage after colonic cancer surgery.* Colorectal Dis, 2012. **14**(10): p. e661-7.
12. Pommergaard, H.C., et al., *Preoperative risk factors for anastomotic leakage after resection for colorectal cancer: a systematic review and meta-analysis.* Colorectal Dis, 2014. **16**(9): p. 662-71.
13. McDermott, F.D., et al., *Systematic review of preoperative, intraoperative and postoperative risk factors for colorectal anastomotic leaks.* Br J Surg, 2015. **102**(5): p. 462-79.
14. Nerstrom, M., et al., *Therapeutic improvement of colonic anastomotic healing under complicated conditions: A systematic review.* World J Gastrointest Surg, 2016. **8**(5): p. 389-401.
15. Mukherjee, K., S.L. Kavalukas, and A. Barbul, *Nutritional Aspects of Gastrointestinal Wound Healing.* Adv Wound Care (New Rochelle), 2016. **5**(11): p. 507-515.
16. van Praagh, J.B., et al., *Intestinal microbiota and anastomotic leakage of stapled colorectal anastomoses: a pilot study.* Surg Endosc, 2016. **30**(6): p. 2259-65.
17. Bachmann, R., et al., *Novel insight into the role of microbiota in colorectal surgery.* Gut, 2017. **66**(4): p. 738-749.
18. Marjanovic, G. and U.T. Hopt, *[Physiology of anastomotic healing].* Chirurg, 2011. **82**(1): p. 41-7.
19. DiPietro, L.A., *Wound healing: the role of the macrophage and other immune cells.* Shock, 1995. **4**(4): p. 233-40.
20. Rijcken, E., et al., *Growth factors and gastrointestinal anastomotic healing.* J Surg Res, 2014. **187**(1): p. 202-10.

21. Weidmann, H., et al., *The plasma contact system, a protease cascade at the nexus of inflammation, coagulation and immunity.* Biochim Biophys Acta, 2017. **1864**(11 Pt B): p. 2118-2127.
22. Del Rio, J.V., D.E. Beck, and F.G. Opelka, *Chronic perioperative steroids and colonic anastomotic healing in rats.* J Surg Res, 1996. **66**(2): p. 138-42.
23. Mantzoros, I., et al., *The effect of insulin-like growth factor I on healing of colonic anastomoses in cortisone-treated rats.* Dis Colon Rectum, 2006. **49**(9): p. 1431-8.
24. Inglin, R.A., et al., *Insulin-like growth factor I improves aspects of mycophenolate mofetil-impaired anastomotic healing in an experimental model.* Br J Surg, 2008. **95**(6): p. 793-8.
25. Zacharakis, E., et al., *Effect of IGF-I on healing of colonic anastomoses in rats under 5-FU treatment.* J Surg Res, 2008. **144**(1): p. 138-44.
26. Wu, M.C., et al., *The receptor for complement component C3a mediates protection from intestinal ischemia-reperfusion injuries by inhibiting neutrophil mobilization.* Proc Natl Acad Sci U S A, 2013. **110**(23): p. 9439-44.
27. Witte, M.B. and A. Barbul, *General principles of wound healing.* Surg Clin North Am, 1997. **77**(3): p. 509-28.
28. Engelhardt, E., et al., *Chemokines IL-8, GROalpha, MCP-1, IP-10, and Mig are sequentially and differentially expressed during phase-specific infiltration of leukocyte subsets in human wound healing.* Am J Pathol, 1998. **153**(6): p. 1849-60.
29. Martin, P. and S.J. Leibovich, *Inflammatory cells during wound repair: the good, the bad and the ugly.* Trends Cell Biol, 2005. **15**(11): p. 599-607.
30. Leoni, G., et al., *Wound repair: role of immune-epithelial interactions.* Mucosal Immunol, 2015. **8**(5): p. 959-68.
31. Xavier, R.J. and D.K. Podolsky, *Unravelling the pathogenesis of inflammatory bowel disease.* Nature, 2007. **448**(7152): p. 427-34.
32. Fournier, B.M. and C.A. Parkos, *The role of neutrophils during intestinal inflammation.* Mucosal Immunol, 2012. **5**(4): p. 354-66.
33. Tauzin, S., et al., *Redox and Src family kinase signaling control leukocyte wound attraction and neutrophil reverse migration.* J Cell Biol, 2014. **207**(5): p. 589-98.
34. Ortega-Gomez, A., M. Perretti, and O. Soehnlein, *Resolution of inflammation: an integrated view.* EMBO Mol Med, 2013. **5**(5): p. 661-74.
35. Chen, G.Y. and G. Nunez, *Sterile inflammation: sensing and reacting to damage.* Nat Rev Immunol, 2010. **10**(12): p. 826-37.
36. Murray, P.J. and T.A. Wynn, *Protective and pathogenic functions of macrophage subsets.* Nat Rev Immunol, 2011. **11**(11): p. 723-37.
37. Barron, L. and T.A. Wynn, *Fibrosis is regulated by Th2 and Th17 responses and by dynamic interactions between fibroblasts and macrophages.* Am J Physiol Gastrointest Liver Physiol, 2011. **300**(5): p. G723-8.
38. Sindrilaru, A., et al., *An unrestrained proinflammatory M1 macrophage population induced by iron impairs wound healing in humans and mice.* J Clin Invest, 2011. **121**(3): p. 985-97.
39. Murray, P.J., *The primary mechanism of the IL-10-regulated antiinflammatory response is to selectively inhibit transcription.* Proc Natl Acad Sci U S A, 2005. **102**(24): p. 8686-91.
40. Biswas, S.K. and A. Mantovani, *Macrophage plasticity and interaction with lymphocyte subsets: cancer as a paradigm.* Nat Immunol, 2010. **11**(10): p. 889-96.
41. Scannell, M., et al., *Annexin-1 and peptide derivatives are released by apoptotic cells and stimulate phagocytosis of apoptotic neutrophils by macrophages.* J Immunol, 2007. **178**(7): p. 4595-605.

42. Bratton, D.L. and P.M. Henson, *Neutrophil clearance: when the party is over, clean-up begins.* Trends Immunol, 2011. **32**(8): p. 350-7.
43. Yang, Y.H., et al., *Modulation of inflammation and response to dexamethasone by Annexin 1 in antigen-induced arthritis.* Arthritis Rheum, 2004. **50**(3): p. 976-84.
44. Migaly, J., et al., *Effect of adenoviral-mediated transfer of transforming growth factor-beta1 on colonic anastomotic healing.* Dis Colon Rectum, 2004. **47**(10): p. 1699-705.
45. Dubay, D.A. and M.G. Franz, *Acute wound healing: the biology of acute wound failure.* Surg Clin North Am, 2003. **83**(3): p. 463-81.
46. Thornton, F.J. and A. Barbul, *Healing in the gastrointestinal tract.* Surg Clin North Am, 1997. **77**(3): p. 549-73.
47. Sharefkin, J., et al., *Anastomotic dehiscence after low anterior resection of the rectum.* Am J Surg, 1978. **135**(4): p. 519-23.
48. Goligher, J.C., N.G. Graham, and F.T. De Dombal, *Anastomotic dehiscence after anterior resection of rectum and sigmoid.* Br J Surg, 1970. **57**(2): p. 109-18.
49. Le, Y., et al., *Novel pathophysiological role of classical chemotactic peptide receptors and their communications with chemokine receptors.* Immunol Rev, 2000. **177**: p. 185-94.
50. Babbin, B.A., et al., *Annexin I regulates SKCO-15 cell invasion by signaling through formyl peptide receptors.* J Biol Chem, 2006. **281**(28): p. 19588-99.
51. Rane, M.J., et al., *Formyl peptide receptors are coupled to multiple mitogen-activated protein kinase cascades by distinct signal transduction pathways: role in activation of reduced nicotinamide adenine dinucleotide oxidase.* J Immunol, 1997. **159**(10): p. 5070-8.
52. Perretti, M., *Lipocortin 1 and chemokine modulation of granulocyte and monocyte accumulation in experimental inflammation.* Gen Pharmacol, 1998. **31**(4): p. 545-52.
53. Belisle, B. and A. Abo, *N-Formyl peptide receptor ligation induces rac-dependent actin reorganization through Gbeta gamma subunits and class Ia phosphoinositide 3-kinases.* J Biol Chem, 2000. **275**(34): p. 26225-32.
54. Glogauer, M., J. Hartwig, and T. Stossel, *Two pathways through Cdc42 couple the N-formyl receptor to actin nucleation in permeabilized human neutrophils.* J Cell Biol, 2000. **150**(4): p. 785-96.
55. Roviezzo, F., et al., *The annexin-1 knockout mouse: what it tells us about the inflammatory response.* J Physiol Pharmacol, 2002. **53**(4 Pt 1): p. 541-53.
56. Chodniewicz, D. and D.V. Zhelev, *Chemoattractant receptor-stimulated F-actin polymerization in the human neutrophil is signaled by 2 distinct pathways.* Blood, 2003. **101**(3): p. 1181-4.
57. Rescher, U., et al., *Functional activation of the formyl peptide receptor by a new endogenous ligand in human lung A549 cells.* J Immunol, 2002. **169**(3): p. 1500-4.
58. VanCompernolle, S.E., et al., *Expression and function of formyl peptide receptors on human fibroblast cells.* J Immunol, 2003. **171**(4): p. 2050-6.
59. Perretti, M., et al., *Endogenous lipid- and peptide-derived anti-inflammatory pathways generated with glucocorticoid and aspirin treatment activate the lipoxin A4 receptor.* Nat Med, 2002. **8**(11): p. 1296-302.
60. Hughes, E.L., et al., *Mast cells mediate early neutrophil recruitment and exhibit anti-inflammatory properties via the formyl peptide receptor 2/lipoxin A4 receptor.* Br J Pharmacol, 2017. **174**(14): p. 2393-2408.
61. Sheikh, M.H. and E. Solito, *Annexin A1: Uncovering the Many Talents of an Old Protein.* Int J Mol Sci, 2018. **19**(4).

62. Leoni, G., et al., *Annexin A1, formyl peptide receptor, and NOX1 orchestrate epithelial repair.* J Clin Invest, 2013. **123**(1): p. 443-54.
63. Leoni, G., et al., *Annexin A1-containing extracellular vesicles and polymeric nanoparticles promote epithelial wound repair.* J Clin Invest, 2015. **125**(3): p. 1215-27.
64. Perretti, M., et al., *Mobilizing lipocortin 1 in adherent human leukocytes downregulates their transmigration.* Nat Med, 1996. **2**(11): p. 1259-62.
65. Solito, E., et al., *A novel calcium-dependent proapoptotic effect of annexin 1 on human neutrophils.* FASEB J, 2003. **17**(11): p. 1544-6.
66. Yauw, S.T., et al., *Systematic review of experimental studies on intestinal anastomosis.* Br J Surg, 2015. **102**(7): p. 726-34.
67. Pommergaard, H.C., et al., *Choosing the best animal species to mimic clinical colon anastomotic leakage in humans: a qualitative systematic review.* Eur Surg Res, 2011. **47**(3): p. 173-81.
68. Reischl, S., et al., *Ac2-26-Nanoparticles Induce Resolution of Intestinal Inflammation and Anastomotic Healing via Inhibition of NF-kappaB Signaling in a Model of Perioperative Colitis.* Inflamm Bowel Dis, 2021.
69. Ulm, K., *Statistische Begutachtung des Antrags auf Genehmigung eines Tierversuchsvorhabens nach § 8 Abs. 1 des Tierschutzgesetzes mit dem Titel: „Untersuchung der Wirkung Annexin A1 haltiger Nanopartikel auf die intestinalen Wund- und Anastomosenheilung im Rahmen entzündlicher Prozesse"*. 2017, Klinikum rechts der Isar, Institut für Medizinische Informatik, Statistik und Epidemiologie: München.
70. Miltschitzky, J.R.E., et al., *Intestinal anastomotic healing models during experimental colitis.* Int J Colorectal Dis, 2021. **36**(10): p. 2247-2259.
71. Wirtz, S., et al., *Chemically induced mouse models of intestinal inflammation.* Nat Protoc, 2007. **2**(3): p. 541-6.
72. Wirtz, S., et al., *Chemically induced mouse models of acute and chronic intestinal inflammation.* Nat Protoc, 2017. **12**(7): p. 1295-1309.
73. Gonçalves, F.d.C., et al., *Characterization of acute murine dextran sodium sulfate (DSS) colitis: severity of inflammation is dependent on the DSS molecular weight and concentration.* Acta Scientiae Veterinariae, 2013. **41**: p. 01-09.
74. Fukuchi, S.G., et al., *Influence of 5-fluorouracil on colonic healing and expression of transforming growth factor-beta 1.* J Surg Res, 1999. **84**(2): p. 121-6.
75. Kozlowski, C., et al., *An entirely automated method to score DSS-induced colitis in mice by digital image analysis of pathology slides.* Dis Model Mech, 2013. **6**(3): p. 855-65.

Project related publications

Intestinal anastomotic healing models during experimental colitis (Miltschitzky, Clees et al. 2021)

Published in *International Journal of Colorectal Disease (IJCD)* on August 28, 2021.

Authors: Miltschitzky, J. R. E., Clees, Z., Weber, M. C., Vieregge, V., Walter, R. L., Friess, H., Reischl, S., Neumann, P. A.

This method-focused publication first highlights the necessity for a standardized mouse model to research anastomotic healing under inflammatory conditions, then presents the model developed during this thesis with detailed instructions for all procedures and scores. For validation purposes, data from experiments conducted by Z. Clees and M. C. Weber is included.

Ac2-26-Nanoparticles Induce Resolution of Intestinal Inflammation and Anastomotic Healing via Inhibition of NF-κB Signaling in a Model of Perioperative Colitis (Reischl, Lee et al. 2021)

Published in *Inflammatory Bowel Disease (IBD)* on September 9, 2021.

Authors: Reischl, S., Lee, J. H., Miltschitzky, J. R. E., Vieregge, V., Walter, R. L., Twardy, V., Kasajima, A., Friess, H., Kamaly, N., Neumann, P. A.

This publication presents the results of experiments to analyze the effect of ANXA1 on resolution of inflammation in a surgical context. Included are results using Anxa1-knockout mice, the study of perioperative treatment with Ac2-26 loaded NPs on our mouse model as well as a whole-genome RNA sequencing proving modulation of NF-κB signaling.

Full list of materials

Surgical instruments				
Name	Manufacturer name	Supplier	REF No.	#
Fine needle holder	Round Handled Needle Holder	FST	12075-12	1
Medium sized needle holder	Castroviejo Needle Holder	FST	12565-14	1
Coarse needle holder	CRILE-WOOD (BABY) DUROGRIP(R) 150 MM straight needle holder	Aesculap	BM013R	1
Scissors	Fine Scissors - Sharp	FST	14060-11	1
Fine pincers	Student Dumont #5 Forceps	FST	91150-20	2
Coarse pincers	Micro-Adson-Pinzette	Peha-instrument	9910671	1
Wound retractor	Alm Retractor with Blades	FST	17009-08	1
Bulldog serrefine clamp	Bulldog Serrefines	FST	18051-50	2
Biopsy punch	Disposable Biopsy Punch	pfm medical ag	48501	1
Ear punch	Napox		KN-292-2	1

Appendix table 1: Surgical instruments

Syringes and similar materials				
Name	Supplier	REF	#	Vol/Size
Injekt Luer Solo	B.Braun	4606051V	1	5ml
Sterican	Braun	4657705	1	27Gx3/4”
Sterican	Braun	4657519	1	20Gx1 1/2”
Disposable Scalpel	Feather		1	22 blade
Vasofix Braunüle	Braun	4268113B	1	G20 1.10x33 mm

Appendix table 2: Syringes and similar materials

VIII Investigation of the Effect of Nano Particles Containing Ac2-26 on Intestinal Inflammation in the Context of Inflammatory Processes in the Intestine

Consumables				
Name	Supplier	REF	#	Vol/Size
Vliwasoft(R) Split dressing	Lohmann&Rauscher	12 099	1	2 pcs
Cotton applicator	Nobamed	974205	1	2 pcs
Haemoccult SENSA	Beckman Coulter	395034	1	40 pcs a 30 test-cards a 2 tests
Leukofix	BSN medical	02138-00	1	6 pcs
Tissue culture dish	Falcon	353003	1	

Appendix table 3: Consumables

Sutures						
Usage	Size	Name	Supplier	Needle specs	Length	REF
Peritoneum Skin	5-0	Prolene	Ethicon	2xC1 13 mm 3/8c VISI-BLACKTM	75 cm	EH7477H
Colon	9-0	Vicryl	Ethicon(R)	BV130-5 6.5 mm 3/8c MultiPassTM	15 cm	V239
Tied suture	4-0	Vicryl	Ethicon(R)	SUTUPAKTM	5x70 cm	V1214

Appendix table 4: Suture materials

Solutions and antiseptics			
Name	Supplier	REF/PZN	Vol/Size
Octeniderm(R) far-blos	Schülke & Mayr GmbH	PZN-3673202	250 ml
NaCl 0.9%	B. Braun Melsungen GmbH		100 ml
G-40%	B. Braun Melsungen GmbH		10 ml

Appendix table 5: Solutions and antiseptics

Software tools used for statistical analysis

T-tests of the weight distribution presented in 3.3.1 were calculated using the “T.TEST” function in Microsoft® Excel® for Microsoft 365 MSO (Version 2111 Build 16.0.14701.20240) 32-bit.

Correlation coefficients, confidence intervals, single t-tests and Mann-Whitney-U as presented in the other paragraphs were calculated using GraphPad Prism® 5 for Windows (Version 5.01).

Acknowledgements

Although I have written this thesis completely on my own and without help from a third party, research is teamwork and so there are several persons and a few institutions I would like to give my heartfelt gratitude to for their support, guidance and feedback:

The first thanks go out to my mentors on the way to this thesis: PD Dr. Philipp-Alexander Neumann, Prof. Dr. Güralp Ceyhan, Prof. Dr. Hana Algül and Dr. Stefan Reischl. Thank you for coaching me through the years to two successful publications and the completion of this thesis! To the other co-authors of the project-related publications mentioned here, especially Zoé Clees, Marie-Christin Weber, Vincent Vieregge and Robert Walter: thank you for the great collaboration on the experiments that eventually made successful publication of our papers and this thesis possible! Thanks to Lucia Gampl for her excellent support as technical assistant during my lab experiments. Thanks to Dr. Nazila Kamaly for providing us with the nanoparticles we needed for our experiments. Thanks to Dr. Asma Nusrat and to Dr. Charles Parkos for hosting me in their Ann Arbor lab for two months and for teaching me part of the methodology needed for this work.

I must also give a big thank you to the *Hanns-Seidel-Stiftung*: for the important skills I could learn in your seminars over the years and for the financial scholarship without which I could probably not have studied medicine at all. I am also grateful to the *Else Kröner-Fresenius-Stiftung* for funding my twelve months of full-time research at TUM.

Last but not least, to my love Charly: thank you for your understanding, for the hours, days and months you let me spend on my work instead of with you without a word of complaint – and for always being there for me when I need you.